Mineralium Deposita
https://doi.org/10.1007/s00126-024-01341-9

ARTICLE

Polymetallic vein formation through fluid flashing at the Sunnyside intermediate-sulfidation epithermal deposit, Colorado, USA

Mario A. Guzman[1] · Thomas Monecke[1] · T. James Reynolds[1,2]

Received: 6 December 2023 / Accepted: 3 December 2024

Abstract

Sunnyside is a well-preserved Miocene polymetallic vein deposit located in the Western San Juan Mountains of Colorado, USA. The steeply dipping veins extend vertically for ~ 600 m and can be traced laterally over a combined length of ~ 2100 m. Fracture-controlled fluid flow dominated during the pre-ore stage. Subsequent ore deposition along major extensional structures took place at far-from-equilibrium conditions resulting in the formation of ore mineral dendrites in a silica matrix that was originally noncrystalline. Recrystallization of the noncrystalline silica to quartz caused extensive microtextural modification of the veins during and after the ore-stage. Microtextural evidence suggests that essentially all quartz in the ore-stage veins originated from a noncrystalline silica precursor. The deposition of ore mineral dendrites and noncrystalline silica is interpreted to have occurred during repeated fluid flashing events over the lifetime of the hydrothermal system. A period of quasi steady-state fluid flow occurred during the post-ore stage resulting in the formation of gangue minerals in open spaces in the veins. Fluid inclusion evidence suggests that the veins at Sunnyside formed at the transition between the epithermal and porphyry environments at ~ 1300–1900 m below the paleowater table at temperatures ranging up to ~ 345 °C.

Introduction

Intermediate-sulfidation epithermal deposits are a distinct group of precious and base metal deposits formed in subduction-related arc settings and post-collisional orogenic belts (John et al. 1999; Hedenquist et al. 2000; John 2001; Sillitoe and Hedenquist 2003; Wang et al. 2019). The deposits are commonly associated with porphyritic intrusions suggesting that differentiated magmas may be the source of the ore-forming hydrothermal liquids (Sillitoe 2010). During their ascent into the epithermal environment, the magmatically derived hydrothermal liquids experience extensive fluid-rock interaction (Reed 1997; Einaudi et al. 2003; Sillitoe and Hedenquist 2003) and possible mixing with ambient meteoric waters (Simmons et al. 1988; Vikre 1989; Koděra et al. 2005; Wang et al. 2019). Ore deposition takes place in the shallow subsurface at depths of less than 1500 m below surface at temperatures ranging up to ~ 300 °C (Buchanan 1981; Hedenquist et al. 2000; Simmons et al. 2005).

Although many comprehensive case studies have focused on the geological and petrographic characteristics of intermediate-sulfidation epithermal deposits (Kamilli and Ohmoto 1977; Simmons et al. 1988; Hayba 1997; Claveria 2001; Camprubí and Albinson 2007; Leary et al. 2016), the mechanisms by which precious and base metal deposition occurs in the shallow subsurface are not fully understood. Previous studies emphasized that metal precipitation in these deposits is typically linked to the occurrence of boiling in the shallow subsurface (Kamilli and Ohmoto 1977; Simmons et al. 1988; Claveria 2001; Albinson et al. 2001; Koděra et al. 2005; Moncada et al. 2012), as the composition of the hydrothermal fluids shifts dramatically during vapor loss (Drummond and Ohmoto 1985; Simmons and Browne 2000). However, differences in the prevailing pressure regimes can result in distinct types of boiling and associated vapor production (Scott and Watanabe 1998; Moncada et al. 2012; Taksavasu et al. 2018; Tharalson et al. 2019, 2023; Slater et al. 2021; Terry et al. 2021; Monecke et al. 2023). A better understanding of the nature of the

Editorial handling: M. Steele-Macinnis

✉ Thomas Monecke
tmonecke@mines.edu

[1] Center to Advance the Science of Exploration to Reclamation in Mining, Department of Geology and Geological Engineering, Colorado School of Mines, 1516 Illinois Street, Golden, CO 80401, USA

[2] FLUID INC., 1401 Wewatta St. #PH3, Denver, CO 80202, USA

Published online: 07 January 2025

boiling processes resulting in the formation of intermediate-sulfidation epithermal deposits has important implications for drill targeting during exploration for this deposit type.

This contribution reports on a study conducted on the Sunnyside polymetallic vein deposit in the San Juan Mountains of Colorado. The research focused on the petrographic and textural characteristics of the ores, which have been historically mined for their high base and precious metal contents. In addition to the investigation of vein textures, the fluid inclusion inventory of gangue minerals was surveyed to better constrain the mechanisms of metal deposition and the depth of mineralization below the paleosurface. It is shown that mineralization at Sunnyside can be related to episodic flash vaporization of the hydrothermal liquids at the transition between the epithermal and porphyry environments.

Geological setting

The Sunnyside deposit is located in the Eureka mining camp of the Western San Juan Mountains in Colorado, United States (Fig. 1). The San Juan Mountains are an erosional remnant of the late Eocene to Oligocene Southern Rocky Mountains volcanic field that originally covered an area exceeding 100,000 km^2 stretching from southern Colorado to northern New Mexico (Fig. 1; Lipman 2007). Volcanism in the Southern Rocky Mountains volcanic field occurred because of ignimbrite flareup-style continental arc volcanism developed on thick continental crust during roll back of the subducting Farallon oceanic plate from a flat configuration to a steeper dip (Lipman 2007; Best et al. 2016).

Volcanism in the Southern Rocky Mountain volcanic field commenced as early as 38 Ma by the eruptions of andesitic lavas in the 39-Mile volcanic area (Fig. 1; McIntosh and Chapin 2004). Early erupted large ignimbrites were sourced from calderas located along the present-day Sawatch Range at 37−33 Ma (Lipman 2007). The first major regional ignimbrite is the Wall Mountain Tuff, which formed at 36.9 Ma from a now eroded caldera above the Mount Princeton batholith (Lipman 2007; Lipman and Bachmann 2015). Volcanism migrated southward along the Sawatch Range, resulting in the formation of scattered andesitic volcanic centers in the San Juan region by 35 Ma (Lipman 2007). Following several million years of this precursor volcanism, large ignimbrite eruptions occurred in the southeast San Juan region at the Platoro caldera complex at 29 Ma (Lipman 1975; Steven and Lipman 1976), followed by the 28.4 Ma San Juan and Uncompahgre calderas in the west (Lipman et al. 1973; Lipman 1976). Explosive, caldera-forming, ignimbrite eruptions depositing voluminous dacitic-rhyolitic ash flow sheets persisted until the formation of the Lake City caldera at 23 Ma (Bove et al. 2001; Lipman 2007), which is also located in the western San Juan region. Volcanic activity related to extension along the Rio Grande rift commenced by ~22 Ma (Lipman et al. 2015). Ignimbrite eruptions in the Southern Rocky Mountain volcanic field were followed by small-scale emplacement of silicic intrusions and effusive eruption of rhyolite flows, with some being as young as 15 Ma (Gonzales 2015). Structural unroofing associated with extension along the Rio Grande rift and deep erosion of the Southern Rocky Mountain volcanic field has exposed broadly synvolcanic batholithic intrusions associated with the ignimbrite centers (Fig. 1; Lipman 2007).

Polymetallic vein deposits of the Eureka mining camp (Burbank 1951; Burbank and Luedke 1969) are located within the Eureka graben (Fig. 2). Mineralization is hosted by the Silverton Volcanics, which accumulated within and adjacent to the 28.4 Ma San Juan and Uncompahgre calderas after their collapse, but before subsidence of the 27.6 Ma Silverton caldera (Lipman et al. 1973; Lipman 1976). The polymetallic vein deposits, however, are younger than the Crystal Lake Tuff sourced from the 27.6 Ma Silverton caldera and the Sunshine Peak Tuff of the 22.9 Ma Lake City caldera (Casadevall and Ohmoto 1977). Rb/Sr dates by Casadevall and Ohmoto (1977) suggest that Sunnyside may be as young as 13.0−16.6 Ma. Deposits within the Eureka camp (Fig. 2) include the Sunnyside deposit (Burbank 1951; Blood 1968; Casadevall and Ohmoto 1977; Langston 1978), which is the focus of this study, as well as the Gold King (Burbank 1951; Taylor 1988; Koch 1990), Scotia-Vanderbilt (Standen and Kyle 1985), and several smaller deposits (Ransome 1901; Burbank and Luedke 1969; Waegli 1979; Bove et al. 2007).

The Eureka graben extends from the northeastern sector of the Silverton caldera to the western rim of the Lake City caldera (Fig. 2). It varies in width from 1.5 km across near the margin of the Silverton caldera to 2 km near the Lake City caldera (Burbank 1951; Burbank and Luedke 1969). The polymetallic veins of the Sunnyside deposit are clustered near the intersection of the Sunnyside fault that borders the Eureka graben in the northwest and the Ross Basin fault that crosscuts the Eureka graben (Fig. 2; Burbank 1933; Burbank 1951; Burbank and Luedke 1969; Casadevall and Ohmoto 1977; Koch 1990).

Deposit geology

Discovered in 1873, mining at Sunnyside was conducted intermittently between 1874 and 1938 (Blood 1968). Revival of the Sunnyside mine started in 1959 with the extension of the American Tunnel from the Gold King mine (Blood 1968), located ~3 km to the southwest of Sunnyside. Construction of the American Tunnel undercutting the Sunnyside mine workings resulted in a second mining boom as the tunnel effectively drained the mine workings and provided a cost-efficient haulage way for underground production. Mining

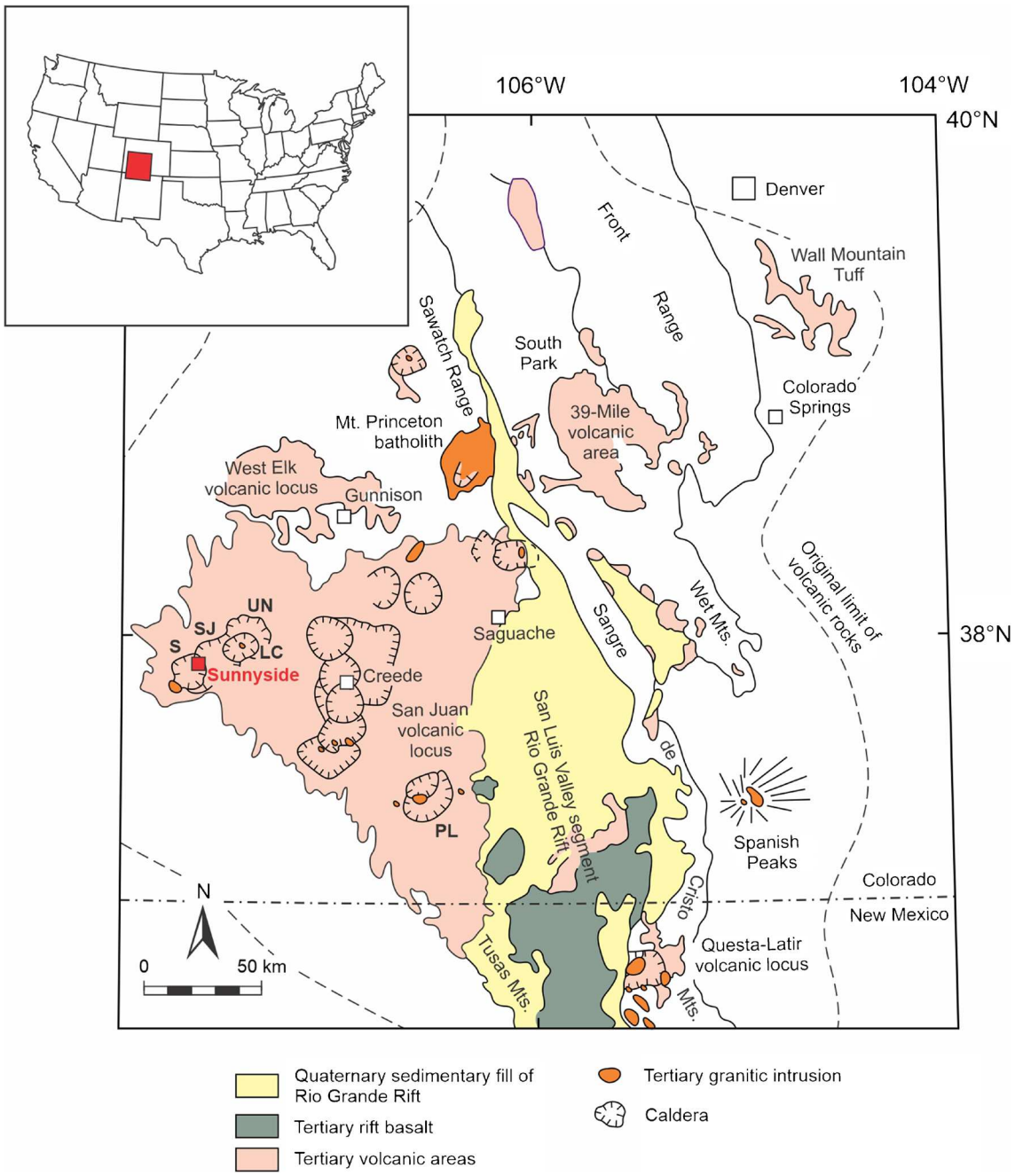

Fig. 1 Geological map of the Eocene to Oligocene Southern Rocky Mountains volcanic field in southwestern Colorado (modified from Lipman 2007), showing ignimbrite calderas, caldera-related granitic intrusions, and the inferred original extent of nearly continuous mid-Tertiary volcanic cover. The map also gives the locations of the Sunnyside deposit (red). Abbreviations of major calderas mentioned in the text: LC Lake City, PL Platoro, S Silverton, SJ San Juan, UN Uncompahgre

at Sunnyside came to a halt due to a major accident in 1978 during which Emma Lake located above the mine workings broke through resulting in the flooding of the Sunnyside mine (Geology Staff Sunnyside Gold Corporation 1988). Production resumed in 1982 and continued until the final mine closure in 1991. Between 1902 and 1987, the Sunnyside mine produced over 6.2 million metric tons of ore for a total of 0.81 million ounces Au and 14.9 million ounces Ag. In addition, 252,000 metric tons of Zn, 180,000 metric tons of Pb, and 18,000 metric tons of Cu were produced (Bartos 1993). In its heyday, Sunnyside was the fifth largest gold producer in the U.S. (Casadevall and Ohmoto 1977).

The Sunnyside deposit is comprised of a series of steeply dipping veins (Fig. 3). Most of the veins strike north-east

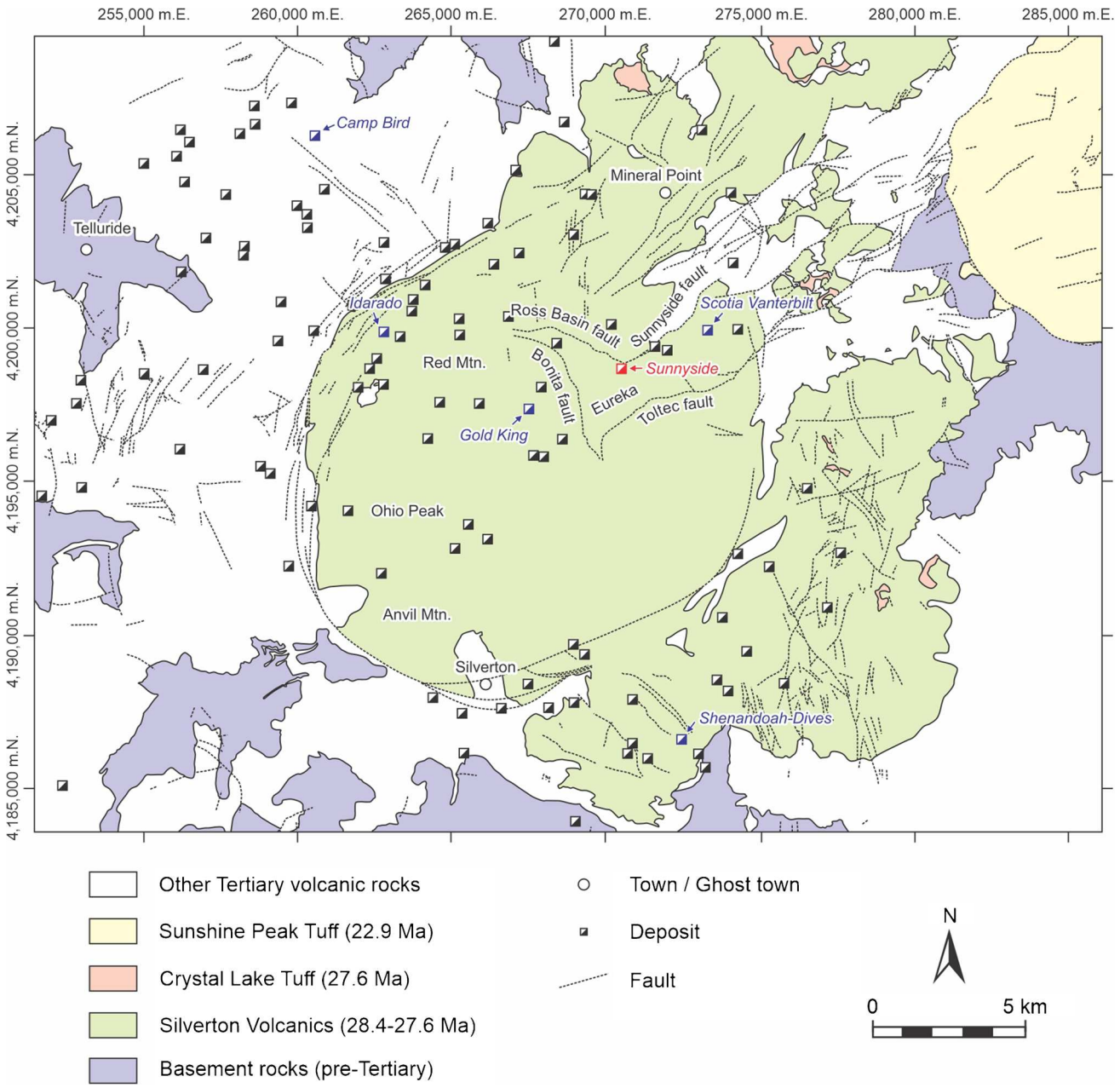

Fig. 2 Regional geological map showing the location of the Sunnyside deposit (red) in the Eureka graben near the structural margin of the Silverton caldera. Other intermediate-sulfidation deposits in the area discussed in the text are highlighted. Quaternary deposits not shown. Map based on Lipman (1976) and Yager and Bove (2002)

paralleling the bounding faults of the Eureka graben (Ransome 1901; Burbank 1933, 1951; Blood 1968). Mineralization extends vertically for ~600 m from 3250 m above sea-level (msl), which is the elevation of the American Tunnel, to 3840 msl. The vein system can be traced laterally over a combined length of ~2100 m. Individual veins at Sunnyside range from <1 to 25 m in width (Ransome 1901; Burbank 1933, 1951; Casadevall and Ohmoto 1977). Veins such as the Belle Creole, No Name, Sunnyside, and Washington outcrop prominently on surface and attracted much of the early mining activity at Sunnyside. In contrast, other important veins such as the 1900, 2150, 2250, and Little Mary veins have little or no surface expression (Casadevall and Ohmoto 1977; Geology Staff Sunnyside Gold Corp. 1988). The veins are offset by late, north-trending faults that show no relationship with earlier structural trends of the Eureka graben (Langston 1978).

The polymetallic veins at Sunnyside are hosted by lavas and associated volcaniclastic rocks of the Burns and Henson members of the Silverton Volcanics. Porphyritic dark-gray to dark-green andesite or rhyodacite of the lower section of the

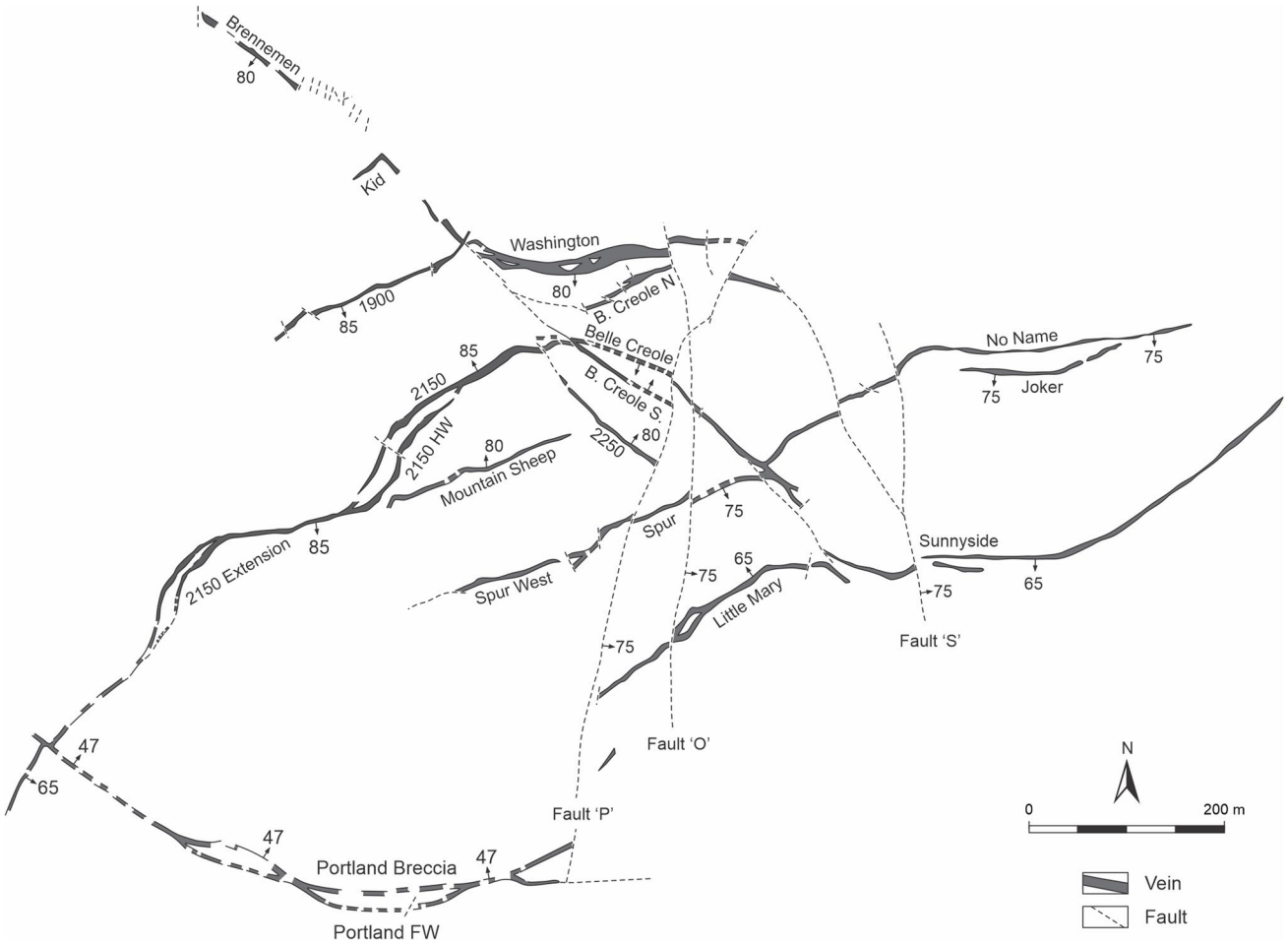

Fig. 3 Geologic plan of the Sunnyside deposit showing the distribution of polymetallic veins and faults on F level at an elevation of 3528 msl (modified from Geology Staff Sunnyside Gold Corporation 1988)

Burns Member occur in the deeper part of the deposit. They are overlain by quartz latite lavas with minor intercalated tuffaceous deposits and flow breccias of the upper section of the Burns Member, which form the principal host to the polymetallic veins (Burbank and Luedke 1969; Casadevall and Ohmoto 1977). The volcanic rocks of the Burns Member are overlain by pyroxene-phyric andesite lavas that interfinger with tuffs and breccia of the Henson Member (Burbank 1951; Burbank and Luedke 1969; Lipman 1976; Langston 1978). The pyroxene-phyric andesite lavas outcrop extensively on surface at Sunnyside (Casadevall and Ohmoto 1977).

The volcanic rocks hosting the polymetallic veins of the Sunnyside deposit have been affected by regional alteration (Burbank 1960; Burbank and Luedke 1969; Casadevall and Ohmoto 1977; Langston 1978). Below the deposit, the volcanic rocks have been overprinted by pervasive alteration resulting in abundant quartz, sericite, and pyrite. Upward within the volcanic succession, the intensity of this alteration style decreases, giving away to an alteration association that is predominated by epidote, chlorite, pyrite, and minor sericite. This alteration assemblage dominates from the base of the deposit at the level of the American Tunnel to surface (Casadevall and Ohmoto 1977).

Diamond drill hole B-1 collared from the American Tunnel to a depth of 2640 msl provided critical information on the geology below the Sunnyside deposit. Throughout the entire length of the hole, abundant veining occurs within volcanic rocks of the lower section of the Burns Member. Guzman et al. (2023) identified narrow veinlets composed of vitreous, white or light gray quartz at 510–585 m, which corresponds to an elevation of 2665−2740 msl. Petrographically, these narrow veins resembled high-temperature porphyry stockwork veins encountered in shallow- and intermediate-depth porphyry deposits. Based on the occurrence of porphyry stockwork veins in drill hole B-1, Guzman et al. (2023) hypothesized that Sunnyside is an example of an intermediate-sulfidation epithermal deposit that is directly connected to a high-level porphyritic pluton. A magnetotelluric survey across the Eureka graben provided additional evidence for the presence of an intrusion below Sunnyside (Rodriguez et al. 2024).

Vein types

Based on consistent crosscutting relationships as well as ore and gangue mineralogy, Casadevall and Ohmoto (1977) distinguished several types of hydrothermal veins (Fig. 4) at the Sunnyside deposit at elevations of 3250–3840 msl. In many cases, the veins have been reopened repeatedly (Burbank 1933; Burbank and Luedke 1969; Casadevall and Ohmoto 1977; Langston 1978) throughout the evolution of the hydrothermal system resulting in texturally complex combinations of the different vein types.

The earliest vein type (Fig. 4a) at Sunnyside consists of pyrite and quartz (Hulin 1929; Burbank 1933; Burbank and Luedke 1969; Casadevall and Ohmoto 1977). These pre-ore stage veins typically are < 5 mm in thickness and are represented by microfractures surrounded by intensely silicified and sericite-altered wall rock. In hand specimens, the gray alteration of the wall rock may be mistaken as vein material. Only locally, the pre-ore stage veins are significantly wider and contain quartz and pyrite crystals that appear to have formed through open space filling (Casadevall and Ohmoto 1977; Langston 1978). Other sulfide minerals can be present but were formed during reopening of the later vein stages (Casadevall and Ohmoto 1977). Some of the best exposed pre-ore stage veins have been documented at the Brenneman vein in the western part of the deposit (Casadevall and Ohmoto 1977).

Four macroscopically distinct types of ore-stage veins are recognized (Burbank 1933; Burbank and Luedke 1969; Casadevall and Ohmoto 1977; Langston 1978). Massive ores (Fig. 4b) are primarily composed of sphalerite and galena (Burbank and Luedke 1969; Casadevall and Ohmoto 1977). Crude banding can be observed in some massive ores (Langston 1978). Anhedral sphalerite and galena crystals in

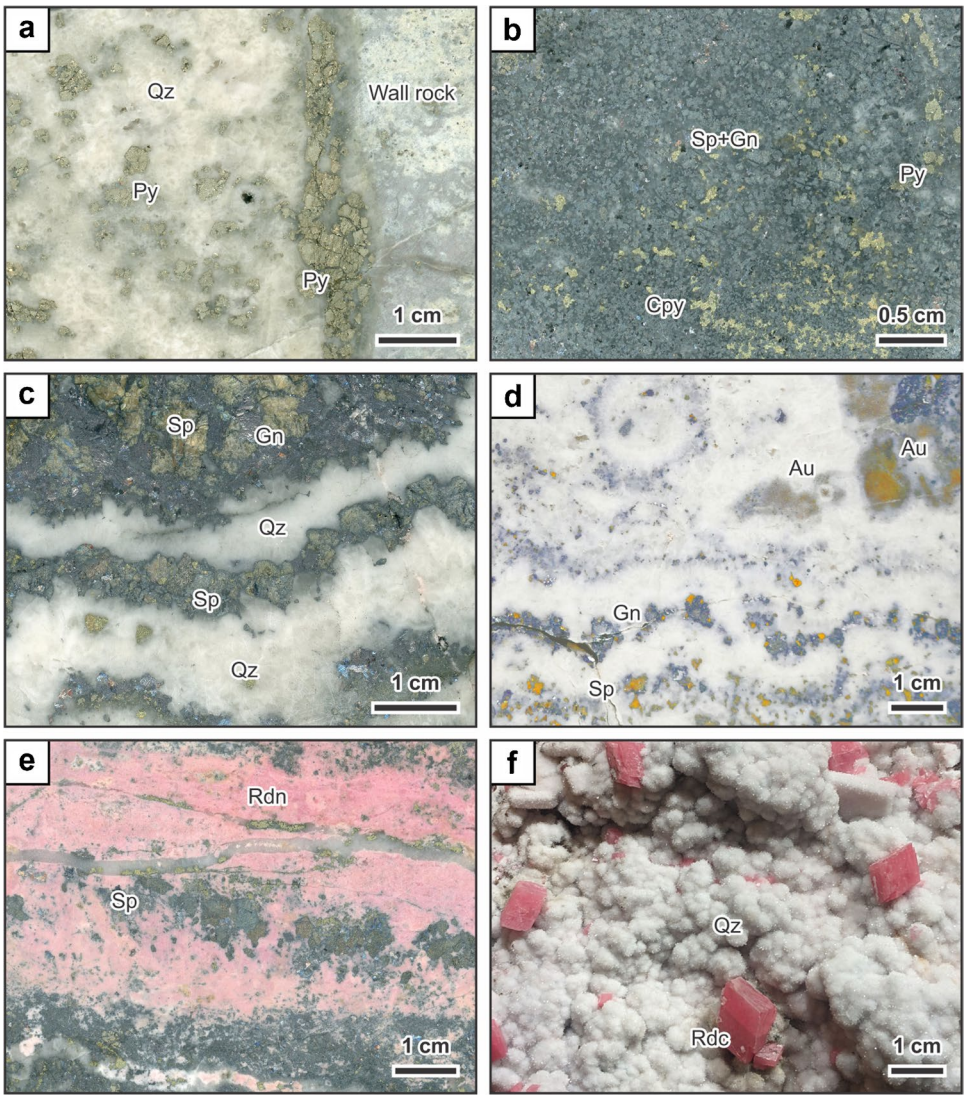

Fig. 4 Hand specimen images of the different vein types occurring at the Sunnyside deposit. **a** Pre-ore stage vein consisting of quartz and pyrite. Pyrite is particularly abundant along the contact to the intensely sericite-altered wall rock. **b** Massive ore consisting of small sphalerite and galena grains set in a silica matrix. Pyrite and chalcopyrite also occur in the massive ore. **c** Banded ore consisting of alternating layers of quartz and ore minerals including sphalerite and galena. **d** Banded quartz vein containing distinct bands of sphalerite and galena. Large native gold aggregates are hosted within the milky white quartz. **e** Manganese ore composed of fine-grained rhodonite. The ore sample contains a band of sphalerite. **f** Post-ore stage rhodochrosite crystals grown into open space within a vuggy cavity lined by drusy quartz crystals. All samples imaged are museum specimens that were not used in the present study. Au native gold, Cpy chalcopyrite, Gn galena, Py pyrite, Qz quartz, Rdc rhodochrosite, Rdn rhodonite, Sp sphalerite

massive ores range from fine- to coarse-grained or form massive aggregates. Minor chalcopyrite and pyrite are present. Aikinite, bornite, and tetrahedrite are locally abundant. The sulfide minerals are commonly set in a white to gray quartz matrix that has a granular texture. Massive ores are abundant throughout the Sunnyside deposit and particularly well developed in the 2150 vein in the southwestern part of the deposit (Casadevall and Ohmoto 1977).

Banded ores show banded and crustiform textures consisting of alternating layers of quartz, sphalerite, and galena (Fig. 4c, d). Minor amounts of chalcopyrite and pyrite are present in all three types of layers in banded ores. Quartz in the banded ores is typically milky white or light gray and microcrystalline to fine-grained. The sulfide minerals in the sphalerite and galena bands are medium- to coarse-grained (Casadevall and Ohmoto 1977). The banded ores commonly contain clasts of wall rock and fragments of earlier formed banded vein material (Langston 1978). Well-developed banded ores have been identified at the Spur vein in the eastern part of the deposit and the 2150 vein in the southwestern portion of Sunnyside (Casadevall and Ohmoto 1977).

Gold ores (Casadevall and Ohmoto 1977; Langston 1978) contain up to 1 cm large native gold grains that are hosted by clear to milky white quartz layers (Fig. 4d). Gold also occurs in association with telluride minerals such as petzite and calaverite (Casadevall and Ohmoto 1977). Pyrite, chalcopyrite, sphalerite, and galena can be present in gold ores. Ores with spectacular native gold have been identified at the 2150 vein, the Spur vein, as well as the Little Mary vein (Casadevall and Ohmoto 1977).

Manganese ores (Fig. 4e) are massive or banded and are composed of fine-grained pyroxmangite or rhodonite, rhodochrosite, and quartz (Ransome 1901; Hulin 1929; Burbank 1933; Burbank and Luedke 1969; Casadevall and Ohmoto 1977). The manganese ores host abundant clasts of older vein material (Langston 1978). Minor amounts of sphalerite, galena, pyrite, and chalcopyrite occur in the manganese ores. Hematite, alabandite, alleghanyite, anhydrite, friedelite, helvite, hübnerite, and tephroite are present in trace quantities (Burbank 1933; Burbank and Luedke 1969; Casadevall and Ohmoto 1977; Langston 1978). The quartz in the manganese ores is typically white to grayish and microcrystalline. Manganese ore accounts for about half of the vein volume of the Washington vein. However, only 5 to 15% of the 2150 and Spur veins are composed of this ore type (Casadevall and Ohmoto 1977).

Post-ore stage veins (Fig. 4f) at Sunnyside consist of quartz, fluorite, calcite, and rhodochrosite (Burbank and Luedke 1969; Casadevall and Ohmoto 1977). Rare euhedral crystals of sphalerite are present. The quartz in these veins is milky white to grayish and commonly drusy in appearance. Fluorite is greenish and can form aggregates that are up to 10 cm in size (Casadevall and Ohmoto 1977). Well-developed examples of post-ore stage veins have been identified at Belle Creole in the central part of the deposit as well as the 2150 vein and the Washington vein (Casadevall and Ohmoto 1977).

Materials and methods

Representative vein samples were obtained from various locations at the Sunnyside deposit, including underground workings and in drill core at elevations ranging from 3245 to 3630 msl (see Supplementary Information). Doubly polished 80-µm-thick sections were prepared to document vein textures and paragenetic relationships in transmitted and reflected light using an Olympus BXM53 optical microscope. Following optical microscopy, the thick sections were carbon coated and inspected using a HC5-LM hot cathode cathodoluminescence (CL) microscope by Lumic Special Microscopes, Germany. The microscope was operated at 14 kV and with a current density of ~ 10 µA mm^{-2} (Neuser 1995). Color images were acquired using a high-sensitivity Teledyne Lumenera Infinity 5–5 digital camera.

Small-scale textural relationships were studied using a TESCAN MIRA3 LMH Schottky field emission-scanning electron microscope equipped with a single-crystal YAG back-scatter electron detector. Imaging was performed at a working distance of 10 mm and an accelerating voltage of 15 kV. Semi-quantitative chemical analyses of minerals were conducted by energy-dispersive X-ray spectroscopy using an attached Bruker XFlash 6|30 silicon drift detector.

In addition to the petrographic investigations, the thick sections were used to study the fluid inclusion inventory of quartz, sphalerite, and fluorite in the different vein types. A limited number of primary fluid inclusion assemblages in pre-ore and post-ore stage samples were studied following the approach of Goldstein and Reynolds (1994). The data was collected to supplement the petrographic observations on the fluid inclusions and do not necessarily constrain the spectrum of conditions that prevailed during these vein stages. A more comprehensive investigation was conducted on the ore-stage samples to reconstruct the depth of mineralization below the paleosurface. All microthermometric investigations were performed using a FLUID INC.-adapted U.S. Geological Survey gas-flow heating and freezing stage that was calibrated using the triple point of CO_2 at −56.6 °C, the triple point of H_2O at 0.0 °C, and the critical point of pure H_2O at 374 °C. Temperatures of phase changes were determined by optical observation or by bracketing to an interval where complete transitions must have occurred using the cycling technique. Estimated precision and accuracy of the measurements are < 0.5 °C at subzero temperatures, and < 5 °C at temperatures > 300 °C. Salinities were calculated according to Bodnar and Vityk (1994).

Petrographic characteristics of vein types

Pre-ore stage

In agreement with the previous studies by Casadevall and Ohmoto (1977) and Langston (1978), the barren pre-ore stage is primarily represented by closely spaced hairline fractures (Fig. 5a). The volcanic host rock is silicified and intensely sericite-altered where the density of hairline fractures is high. However, the alteration is not texturally destructive as faint outlines of former phenocrysts and other volcanic textures can still be recognized in hand specimens and thin sections.

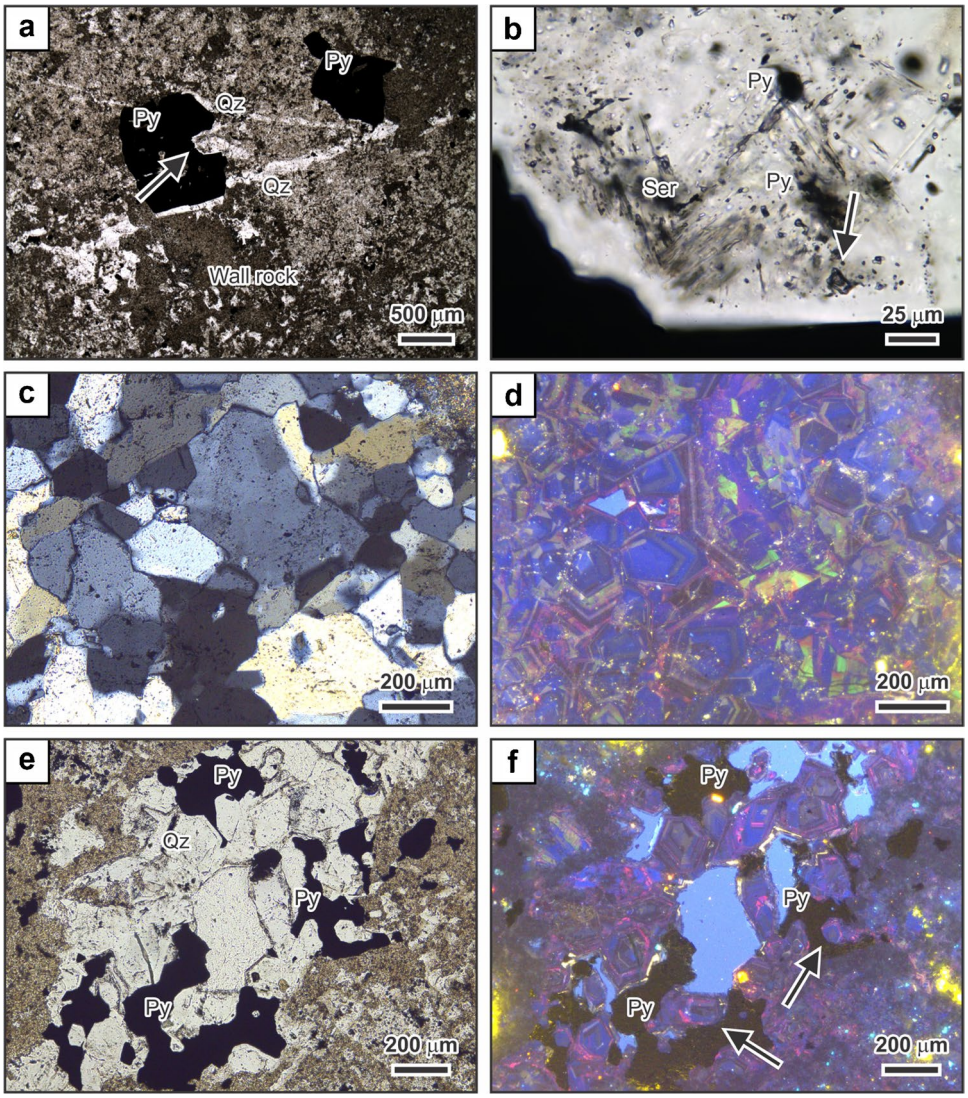

Fig. 5 Textural relationships in pre-ore stage veins at the Sunnyside deposit. **a** Network of hairline fractures that are infilled by quartz. The wall rock transected by the hairline fractures is silicified and intensely sericite-altered. Pyrite occurs throughout the wall rock. Small euhedral quartz crystals occur along the hairline fractures and in cavities in the wall rock (arrow). Plane polarized light. Sample SM-90-2. **b** High-magnification image of the euhedral quartz crystal in Fig. 5a. The core of the crystal contains encapsulated pyrite and abundant primary fluid inclusions (arrow) that are associated with encapsulated flakes of sericite. The textural evidence suggests that quartz, pyrite, and sericite formed contemporaneously. The rim of the crystal is devoid of fluid inclusions, defining core-rim zoning. An assemblage of nine primary inclusions located near the arrow close to the boundary between the cloudy core and the clear rim yielded homogenization temperatures bracketed to 310–320 °C and salinities bracketed to 1.7−2.6 wt% NaCl equiv. Plane polarized light. **c** Quartz crystals in a pre-ore stage vein. Crossed-polarized light. Sample SM-90-1. **d** Corresponding optical cathodoluminescence (CL) image showing that the quartz crystals are euhedral and exhibit oscillatory zoning. **e** Pre-ore stage vein consisting of quartz and pyrite. Contacts of the quartz with the pyrite are scalloped and irregular suggesting that pyrite in this veinlet formed after the quartz. Sample SM-90-3. **f** Corresponding optical CL image showing that the quartz crystals are euhedral and exhibit oscillatory zoning. Pyrite crosscuts the zoning in the euhedral quartz crystals (arrows). Sample SM-90-3. Py pyrite, Qz quartz, Ser sericite

Small quartz crystals (typically < 250 µm in size) occur locally along hairline fractures, in open spaces along fractures, or in vugs within the altered host rocks. The pre-ore stage veins in the samples investigated are mostly < 1.5 mm in width, although some pre-ore stage veins are up to 10 cm wide. Quartz crystals lining open spaces in the pre-ore stage veins may show growth zoning, and commonly exhibit cloudy cores and clearer outer rims (Fig. 5b). Some of the cloudy cores of these quartz crystals contain small, encapsulated sericite flakes and pyrite grains along with abundant liquid-rich fluid inclusions (Fig. 5b). Primary liquid-rich fluid inclusion assemblages are present near the boundaries between the cloudy cores and the clear rims (Fig. 5b). The quartz crystals show a bright blue short-lived CL emission (Fig. 5c–f) that rapidly fades in intensity during continued electron bombardment to yield a long-lived, reddish brown CL emission. Oscillatory growth banding is pronounced in CL images, with individual bands varying in color from red to brown and bluish. Parts of the quartz crystals also exhibit a green CL emission (Fig. 5d).

Pyrite is abundant within the altered host rocks surrounding the pre-ore stage veins. The pyrite forms euhedral crystals or massive aggregates that can be up to several millimeters in size. Pyrite is also present in vugs in the host rocks and as an infill in the pre-ore stage veins overgrowing the earlier euhedral quartz crystals (Fig. 5e, f). Contacts between pyrite and quartz are frequently irregular and scalloped (Fig. 5e) suggesting that not all pyrite and quartz were formed contemporaneously. Pyrite crosscuts zoning in the quartz that is visible in CL (Fig. 5f).

Ore-stage

The various ore types at Sunnyside differ in the relative abundances of ore and gangue minerals and in macroscopic textures. Inspection of thin sections shows that opaque phases present in all ore types occur as irregularly shaped aggregates (Fig. 6). These aggregates, typically consisting of more than one ore mineral, resemble dendrites that have complex, multi-branching shapes. In banded ores, the ore minerals form distinct, undulating bands consisting of dendritic aggregates grown from the vein walls, or from brecciated or curved botryoidal surfaces within the veins towards the center of the veins (Fig. 6a, b). Ore mineral dendrites also occur in gold ores (Fig. 6c, d), massive ores (Fig. 6e), or the manganese ores (Fig. 6f). Sphalerite and galena are the most abundant ore minerals, although chalcopyrite and pyrite dendrites are also common. Native gold occurs as fine-grained (< 250 µm) gold particles that are commonly associated with base metal sulfides (Fig. 6c, d). Individual ore mineral dendrites reach up to 1 cm in size (Fig. 6e). The dendritic nature of the ore minerals may be distinctive in hand sample (Fig. 4d, e), but is commonly more obvious with inspection under the microscope.

The quartz matrix surrounding the ore mineral dendrites is typically fine-grained showing a mosaic or jigsaw texture in crossed-polarized light (Fig. 7a, b). The grain boundaries of the small quartz grains are irregular and interpenetrating. The mosaic quartz appears to have formed because of textural maturation and recrystallization of a noncrystalline silica precursor (Gissler et al. 2024). In some places, transitions between the fine-grained mosaic quartz and polygonal quartz are observed. The grain boundaries of the polygonal quartz are more straight and the grains are uniform in size (Fig. 7c). The transition of mosaic quartz to polygonal quartz involved grain boundary migration and grain coarsening. Both processes resulted in textural changes to the ore mineral dendrites hosted by the quartz such as coarsening of the ore mineral grains and smoothing of the originally highly irregular grain boundaries (Fig. 7c). Mosaic and polygonal quartz in the ore-stage veins do not contain fluid inclusions large enough to be observed with a petrographic microscope. Both quartz types show a short-lived, blue CL emission and lack internal zoning (Fig. 7d). During continued electron bombardment, the CL emission changes to deep brown.

Much of the quartz in the ore-bearing veins forms coarse-grained prismatic crystals showing concentric zoning (Fig. 8a–d). The prismatic crystals have short-lived blue or yellow CL colors (Fig. 8b, d) with the colors gradually changing to a darker yellow or red-brown luminescence during electron bombardment, respectively. However, the prismatic crystals can also be greenish or reddish in CL. The concentric zones are commonly accentuated under CL, with individual zones varying from planar to wavy and round (Fig. 8d). These characteristics indicate that the large prismatic crystals are a product of recrystallization of a noncrystalline precursor (cf. Gissler et al. 2024).

Some of the prismatic grains show zones of feathery texture in crossed-polarized light (Fig. 8e, f). These zones consist of elongate crystal domains that have slightly different extinction angles from each other. The elongate crystal domains are at high angle to the concentric zoning of the prismatic grains. In some cases, the feathery outer domains of the prismatic quartz grains transition into the surrounding quartz matrix. The frayed outer margins of the large prismatic quartz crystals in contact with the surrounding matrix (Fig. 8) suggest that the crystals did not form in open space but represent products of recrystallization from a noncrystalline silica precursor (cf. Gissler et al. 2024).

Manganese ores are massive or consist of colloform bands containing abundant pink, reddish, or brown rhodonite. Microscopically, rhodonite is fine-grained, forming small transparent to translucent tabular crystals. The rhodonite crystals are commonly randomly oriented and hosted

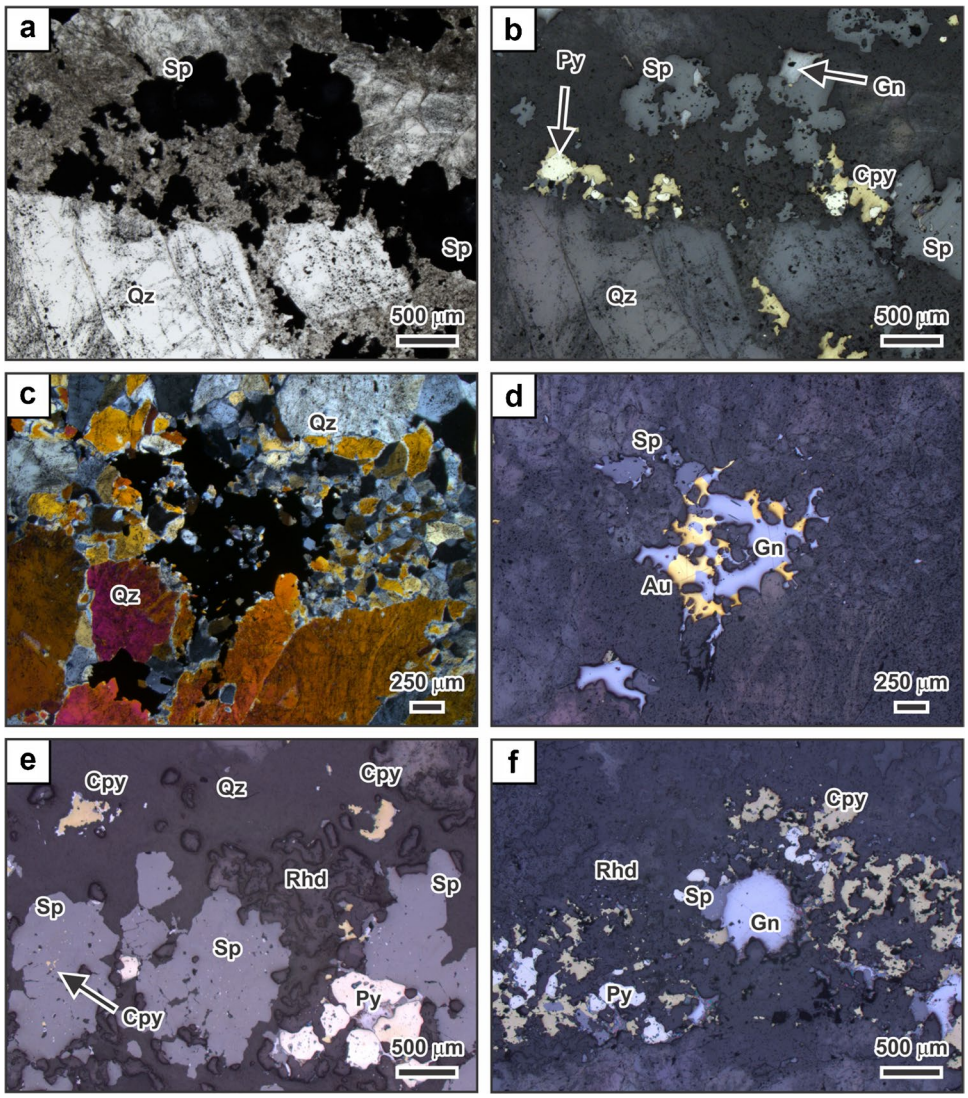

Fig. 6 Ore mineral textures in ore-stage veins from the Sunnyside deposit. **a** Ore containing bands of opaque phases and quartz. The opaque phases form irregular aggregates that resemble dendrites. They are hosted by quartz having a mosaic texture. Plane polarized light. Sample SUN-2150-VN. **b** Corresponding image in reflected light. Pyrite is present together with the ore minerals sphalerite, galena, and chalcopyrite. **c** Ore mineral dendrite hosted by mosaic quartz. Crossed-polarized light. Sample 20-SVTN-007. **d** Corresponding reflected light image showing that the ore mineral dendrite is composed of native gold, galena, and sphalerite. **e** Massive ore containing large sulfide dendrites that are composed of sphalerite, pyrite, and chalcopyrite. The sulfide minerals are hosted by microcrystalline quartz and minor rhodonite. Sphalerite commonly contains very fine-grained encapsulated chalcopyrite. Reflected light. Sample SUN-2150-A. **f** Manganese ore containing a band of sulfide dendrites consisting of galena, chalcopyrite, pyrite, and sphalerite. The matrix contains abundant rhodonite. Reflected light. Sample SUN-2150-D. Au native gold, Cpy chalcopyrite, Gn galena, Py pyrite, Qz quartz, Rhd rhodonite, Sp sphalerite

by quartz. Sphalerite and galena dendrites occur within masses of intergrown rhodonite and quartz (Figs. 4e and 9a).

Some of the manganese ores contain hübnerite intermixed with sulfide minerals. Hübnerite is also present in distinct veinlets crosscutting earlier formed ores (Fig. 9b). In these veinlets, hübnerite occurs as brownish to red bladed crystals forming fan-like aggregates that have nucleated on the vein walls and point towards the center of the veins (Fig. 9b, c). In some cases, radiating aggregates of bladed hübnerite occur that show no preferential orientation with respect to the vein walls (Fig. 9d). Individual hübnerite blades can range up to ~5 mm in size. The bladed hübnerite is hosted by quartz that shows flamboyant textures. Aggregates of flamboyant quartz appear to have nucleated on the hübnerite with the inclusions in the quartz radiating away from the contacts with the hübnerite (Fig. 9c, d).

Prismatic quartz crystals commonly show dark bands resembling primary growth zones (Fig. 10a-c) that are defined by ubiquitous fluid inclusions (Fig. 10d). However, the shape of the bands and their CL characteristics suggest that these crystals were formed by recrystallization of a noncrystalline silica precursor, or by maturation and recrystallization of flamboyant quartz that previously formed from a noncrystalline silica precursor (Fig. 10a). The inclusion-rich bands have textural characteristics that are similar to the recrystallization fronts documented in recrystallized quartz by Gissler et al. (2024). Fluid inclusions defining the recrystallization fronts were trapped during recrystallization (Gissler et al. 2024) and have been referred to as being pseudoprimary by Sander and Black (1988). Pseudoprimary inclusions entrapped during recrystallization of the silica precursor have variable shapes and sizes (cf. Gissler et al. 2024), and many are empty void spaces with highly irregular shapes (Fig. 10d).

Commonly, entire prismatic quartz grains are cloudy and only faint banding can be observed because the prismatic quartz is crosscut by abundant secondary fluid inclusions, with the density of secondary inclusions being so high that

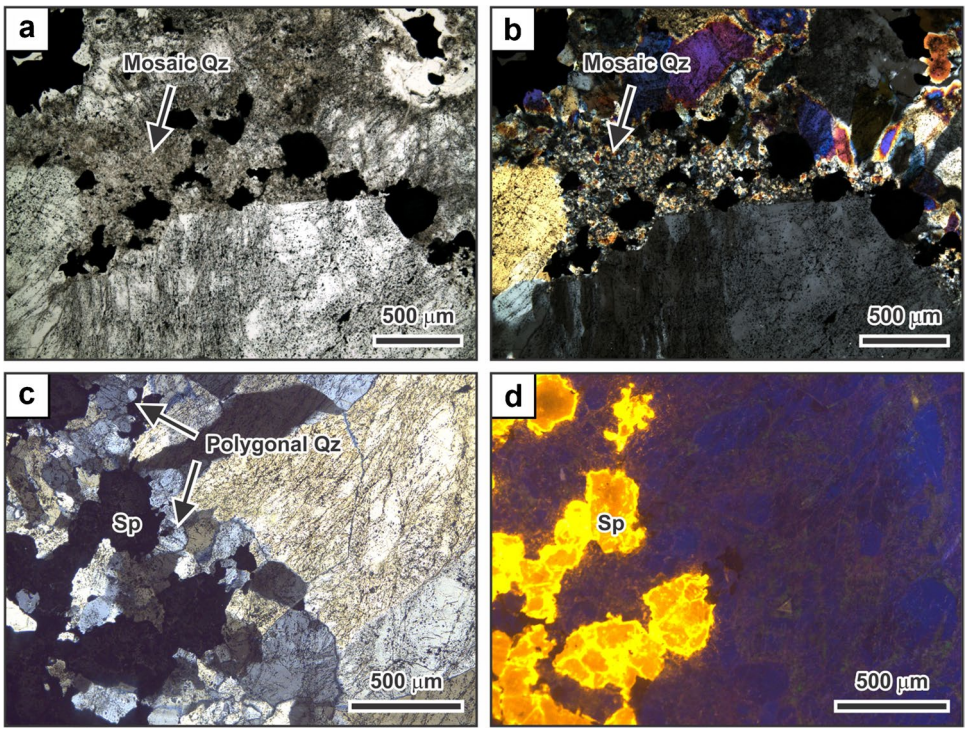

Fig. 7 Textural relationships between quartz and ore minerals in ore-stage veins from the Sunnyside deposit. **a** Fine-grained quartz intermixed with pyrite, sphalerite, and chalcopyrite (opaque phases). Plane polarized light. Sample SUN-2150-VN. **b** Corresponding crossed-polarized light image showing that the quartz exhibits a mosaic texture. The grain boundaries of the small quartz grains are irregular and interpenetrating. **c** Polygonal quartz occurring between the branches of a sphalerite dendrite. The polygonal quartz is characterized by more planar grain boundaries than mosaic quartz and is typically also coarser grained. Crossed-polarized light. Sample PB-13–57. **d** Corresponding cathodoluminescence image of the polygonal quartz occurring between the branches of a sphalerite dendrite. The sphalerite is Fe-poor and exhibits a bright orange to yellow emission during electron bombardment. The polygonal quartz shows a short-lived dark blue emission which changes to deep brown during continued electron bombardment. Qz quartz, Sp sphalerite

individual assemblages cannot be distinguished (Fig. 10e). Identifiable secondary fluid inclusion assemblages occur mostly in clearer cores of the prismatic quartz crystals (Fig. 10f). The secondary fluid inclusions in these assemblages have varying morphologies ranging from irregular to smooth surfaced and oval to equant-shaped, with some approaching negative crystal morphology. Assemblages with more mature shapes (cf. Bodnar et al. 1985) show consistent liquid-to-vapor volumetric proportions (Fig. 10f). In addition to secondary fluid inclusion assemblages that are liquid-rich, many secondary assemblages transecting the prismatic quartz crystals consist entirely of vapor-rich inclusions (Fig. 10g).

Post-ore stage

The post-ore stage veins at Sunnyside are characterized by late euhedral quartz crystals that are distinct from the prismatic quartz formed through recrystallization of a non-crystalline silica precursor, as the late euhedral quartz grew in open spaces (Fig. 11). This late quartz commonly forms drusy crystals that range from several millimeters to centimeters in size protruding into open spaces such as vugs and late fractures (Fig. 11a). The euhedral quartz crystals exhibit a short-lived bluish CL with growth zoning. The CL emission changes to a brownish color during prolonged electron bombardment (Fig. 11b).

Post-ore stage fluorite forms large crystals or intergrown aggregates that are typically greenish, although grayish green and grayish white fluorite also occur. The fluorite aggregates, which can be up to 10 cm in size, can be crosscut by late euhedral, locally drusy quartz (Fig. 11c, d). Crystal faces on the fluorite are commonly etched or corroded. Fluorite exhibits greenish to bluish CL colors and shows complex internal textures including brecciation and etch pits along individual growth zones (Fig. 11d).

Post-ore stage veins include museum-quality rhodochrosite specimens with pink to red rhombohedral or scalenohedral crystals that can be up to several centimeters in size (Fig. 4f). The rhodochrosite crystals are commonly perched upon drusy quartz, indicating that the rhodochrosite is latest in the paragenesis.

In some cases, primary fluid inclusion assemblages were recognized in post-ore stage minerals grown in open space. Rare, late euhedral sphalerite crystals grown on top

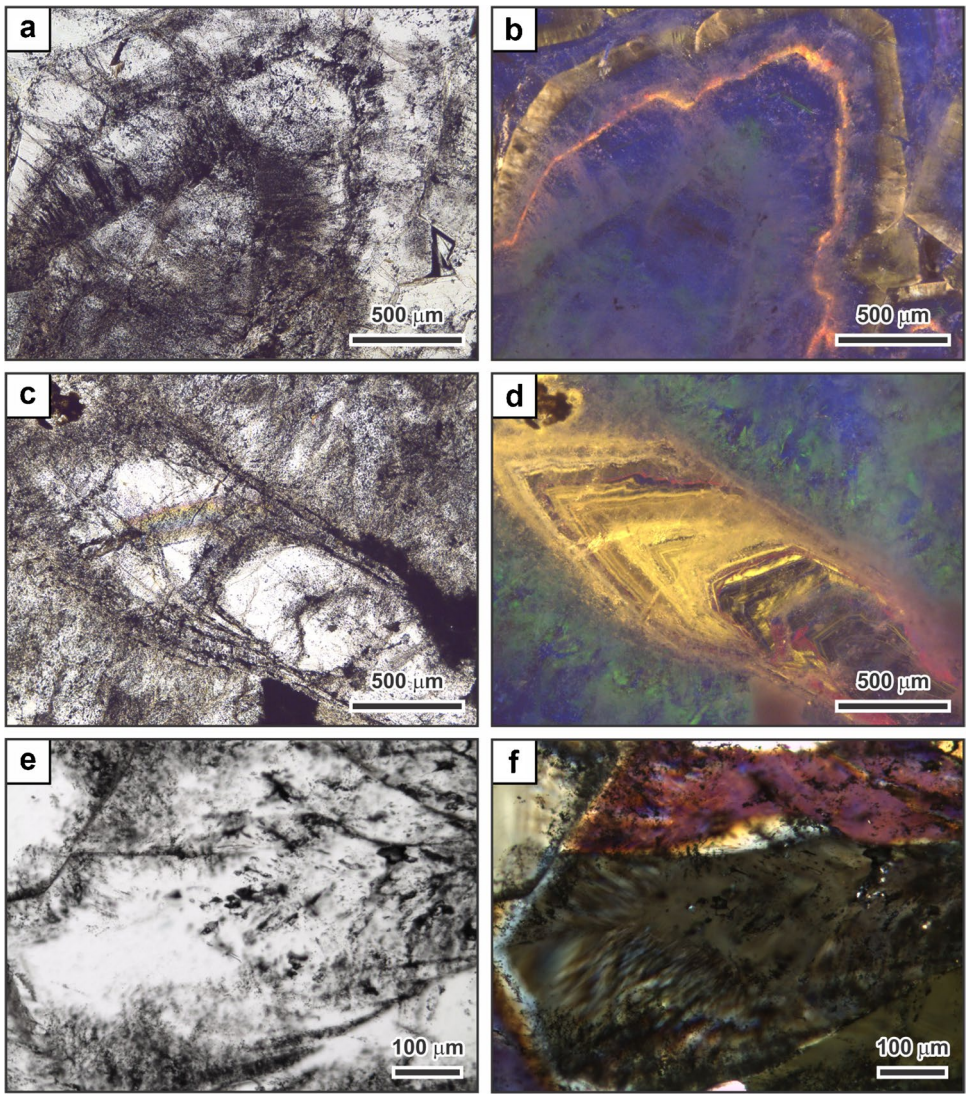

Fig. 8 Textures of quartz in ore-stage veins from the Sunnyside deposit. **a** Large prismatic quartz crystal showing inclusion-rich bands. Inclusions form arrays that radiate outwards from the center of the crystal, but also occur as ubiquitous healed microfractures. Plane polarized light. Sample SUN-2150-D. **b** Corresponding cathodoluminescence (CL) image. The prismatic crystal exhibits a short-lived blue luminescence that changes to a deep brown emission during continued electron bombardment. The outermost zone of the quartz is characterized by a yellow-brown luminescence. A narrow zone of orange CL emission (arrow) is present that is related to the presence of carbonate inclusions. **c** Large prismatic quartz grain set in a matrix of smaller grained quartz crystals. The quartz contains bands that are dark due to abundant inclusions. The outer margin of the crystal is frayed, blending into the surrounding fine-grained quartz (arrows). Plane polarized light. Sample SUN-2150-D. **d** Corresponding CL image. The prismatic quartz crystal exhibits a yellow emission during electron bombardment that fades in intensity over time. The zoning of the crystal is pronounced, with many of the concentric zones being irregular or wavy (arrows) suggesting that the crystal formed through recrystallization of a noncrystalline silica precursor. The prismatic crystal is surrounded by quartz that exhibits greenish and bluish CL colors. **e** Prismatic quartz grain showing a radial arrangement of fluid inclusions. Plane-polarized light. Sample SUN-2150-1. **f** Corresponding crossed-polarized light imaging showing feathery texture within the prismatic quartz. The feathery texture is defined by small elongate quartz splinters that have slightly different extinction angles from each other

of euhedral quartz host primary liquid-rich fluid inclusions defining growth zones (Fig. 12a, b). The late fluorite also contains rare primary liquid-rich fluid inclusions defining growth zones. These commonly occur in association with small rhombic carbonate crystals (Fig. 12c, d) or mica flakes (Fig. 12e).

Microthermometry of fluid inclusions in the ore-stage

Microthermometric investigations were performed on ore-stage samples to constrain the depth of mineralization below the paleosurface. The approach employed here required

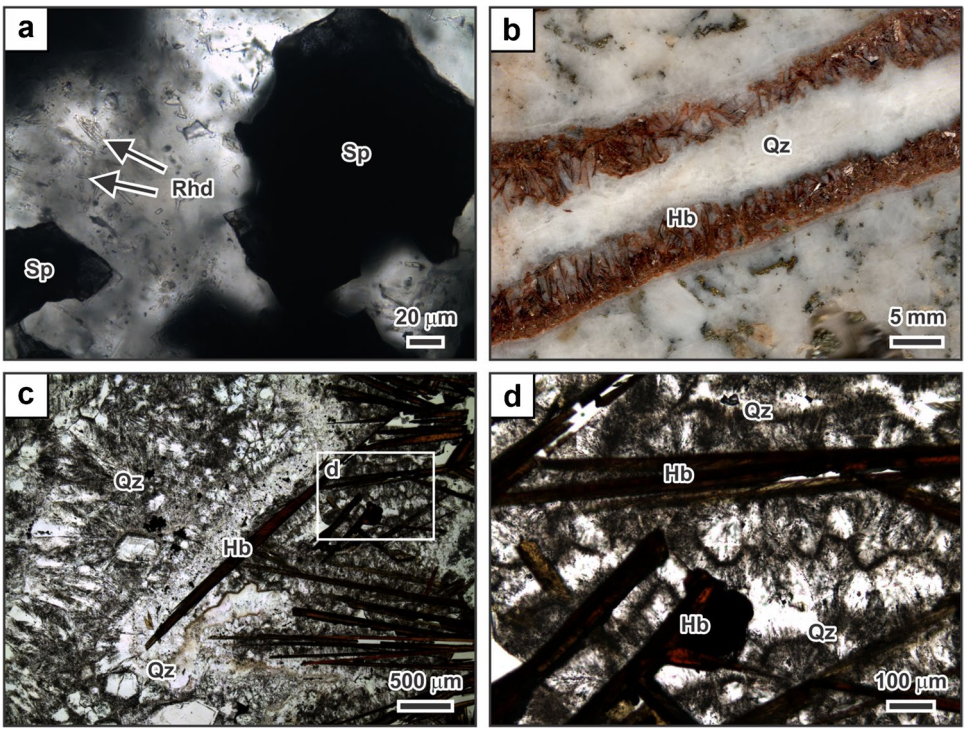

Fig. 9 Textural relationships in ore-stage veins from the Sunnyside deposit containing rhodonite or hübnerite. **a** High-magnification image depicting rhodonite inclusions encapsulated in a matrix of quartz. The matrix hosts sphalerite, which forms part of a larger dendrite. The percentage of rhodonite varies significantly and in some areas little to no quartz is present between the rhodonite crystals. Plane polarized light. Sample 9–20-10. **b** Veinlet composed of hübnerite and quartz cutting earlier vein material. Laths of reddish-brown blades of hübnerite are hosted by white quartz along the margins of the veinlet. Hand specimen image. Sample DS-1–72. **c** Long sheaves of hübnerite hosted by quartz. Plane polarized light. Sample DS-1–72. **d** High-magnification image showing that the hübnerite crystals are suspended in the quartz matrix and show random orientations. Aggregates of flamboyant quartz nucleated on the hübnerite crystals and radiate away from the contacts. Plane polarized light. Sample DS-1–72. Hb hübnerite, Qz quartz, Rhd rhodonite, Sp sphalerite

identification of the highest temperatures of homogenization of liquid-rich inclusion assemblages in samples collected from several mine levels. The petrographic work described above established that minerals of the ore-stage did not form in open spaces. The noncrystalline silica originally deposited did not contain primary fluid inclusions. During the recrystallization to quartz, pseudoprimary fluid inclusions were entrapped in the flamboyant and prismatic quartz crystals, but these inclusions do not yield consistent homogenization temperatures. Meaningful data could only be obtained on secondary fluid inclusion assemblages crosscutting the prismatic quartz crystals. The presence of secondary fluid inclusion assemblages homogenizing at higher temperatures than those recorded from several primary fluid inclusion assemblages in the post-ore stage suggests that the recrystallization from noncrystalline silica to prismatic quartz occurred while the hydrothermal system was active. Lower-temperature secondary fluid inclusion assemblages present in prismatic quartz were not studied here because these assemblages may have been entrapped during the waning stages of the hydrothermal activity or may not be related to the deposit formation at all.

As the homogenization temperatures of fluid inclusions hosted by quartz formed in the epithermal environment can be optically predicted from the liquid-to-vapor volumetric proportions and inclusion shapes (Bodnar et al. 1985), prismatic quartz of the ore-stage samples was systematically surveyed to find equant- to negative crystal-shaped assemblages with consistent liquid-to-vapor volumetric proportions. Once a high-temperature assemblage was recognized, the sample was heated to the temperature of homogenization. The sample was then further surveyed at this temperature within the heating stage to identify possible other assemblages still having bouncing vapor bubbles, which homogenized at a higher temperature. This procedure was repeated until the fluid inclusion assemblages exhibiting the highest, consistent homogenization temperature data in each sample was identified, and the data was then recorded. The final melting point of ice of the highest temperature fluid inclusion assemblages was subsequently collected to determine the salinity.

Table 1 shows the highest temperature fluid inclusions recognized in several ore-stage samples from different mine levels. At G level at an elevation of 3467 msl, the highest

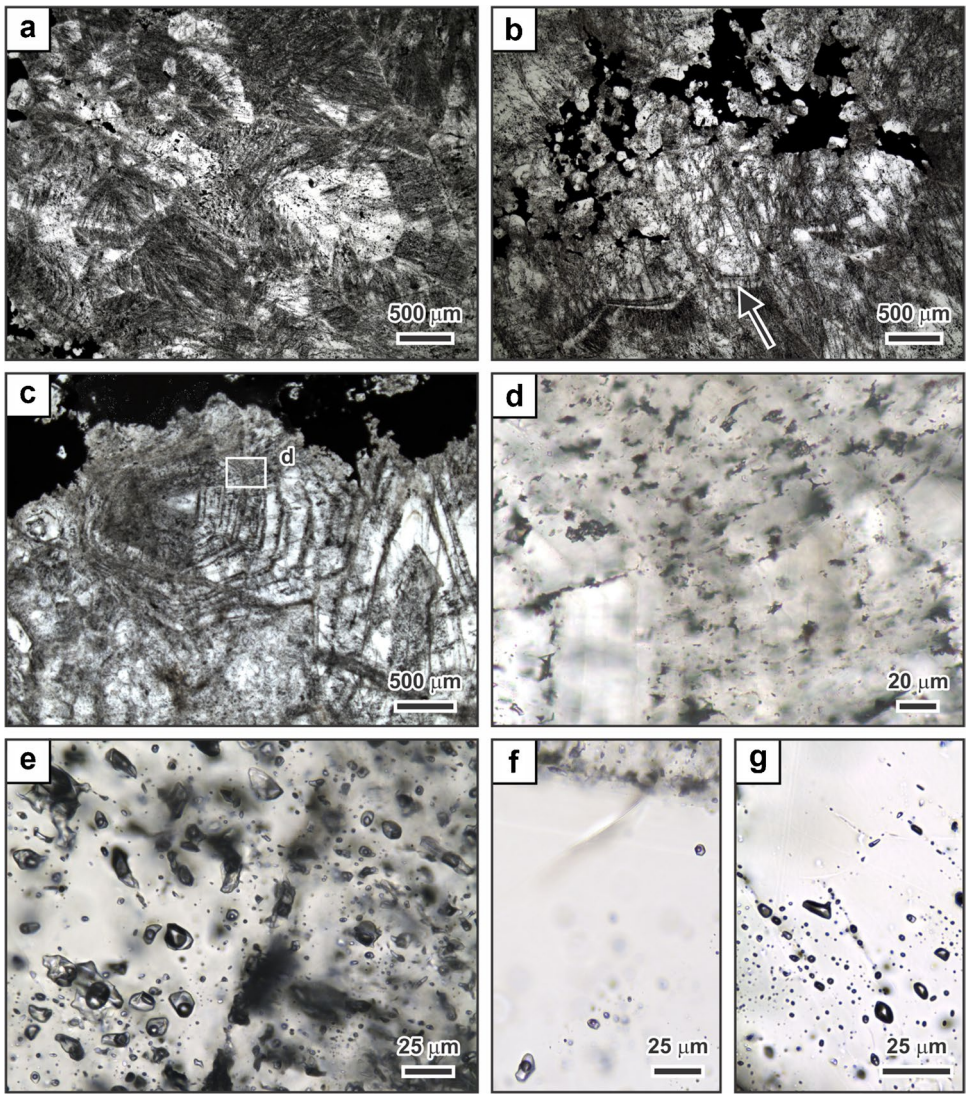

Fig. 10 Photomicrographs of fluid inclusion textures in flamboyant and prismatic quartz within ore-stage veins at the Sunnyside deposit. **a** Dark flamboyant quartz crystal with radiating groups of pseudoprimary fluid inclusions. One large prismatic quartz crystal with a clearer core and radiating groups of inclusions is located in the right part of the image. It is likely that the clear core has resulted from continued recrystallization of a flamboyant quartz crystal and is, therefore, younger than the quartz in the rims (cf. Gissler et al. 2024). Plane polarized light. Sample 20-SVTN-007. **b** Galena dendrite hosted by prismatic quartz crystals. A well-defined recrystallization front (arrow), which resembles a growth band, traverses multiple quartz crystals. This recrystallization front is definitive evidence that the quartz crystals formed through recrystallization of a noncrystalline precursor (cf. Gissler et al. 2024). Plane polarized light. Sample 20-SVTN-007. **c** Two large quartz crystals containing multiple dark recrystallization bands, with the bands being in part curved. The quartz is located next to a band of base metal sulfides. Plane polarized light. Sample SUN-2150-D. **d** High-magnification image of an area shown in the previous image that is characterized by faintly curved recrystallization bands in the prismatic quartz. The bands are defined by arrays of crystallographically controlled pseudoprimary inclusions having highly irregular shapes. Plane polarized light. **e** High-magnification image of secondary fluid inclusions in prismatic quartz. Individual fluid inclusion assemblages cannot be identified. Plane polarized light. Sample SUN-2150-VN. **f** High-magnification image of a healed microfracture of secondary fluid inclusions in a clear core of a prismatic quartz crystal. Inclusions in this assemblage have oval to equant shapes, some approaching negative crystal morphology, with visually consistent liquid-to-vapor volumetric proportions yielding consistent homogenization temperatures of 325–330 °C. The salinity is 1 wt% NaCl equiv. Plane polarized light. Sample SUN-2150-VN. **g** High-magnification image of a secondary plane of vapor-rich inclusions hosted by a prismatic quartz crystal. Sample 7–28-4-2

homogenization temperature in a secondary fluid inclusion trail in prismatic quartz was 325–330 °C. Freezing suggests that the fluid inclusions have a salinity of 1.7−2.6 wt% NaCl equiv. (Table 1). At the F level at 3528 msl, homogenization of fluid inclusions occurred at 340–345 °C. The salinity also was 1.7−2.6 wt% NaCl equiv. Similarly high

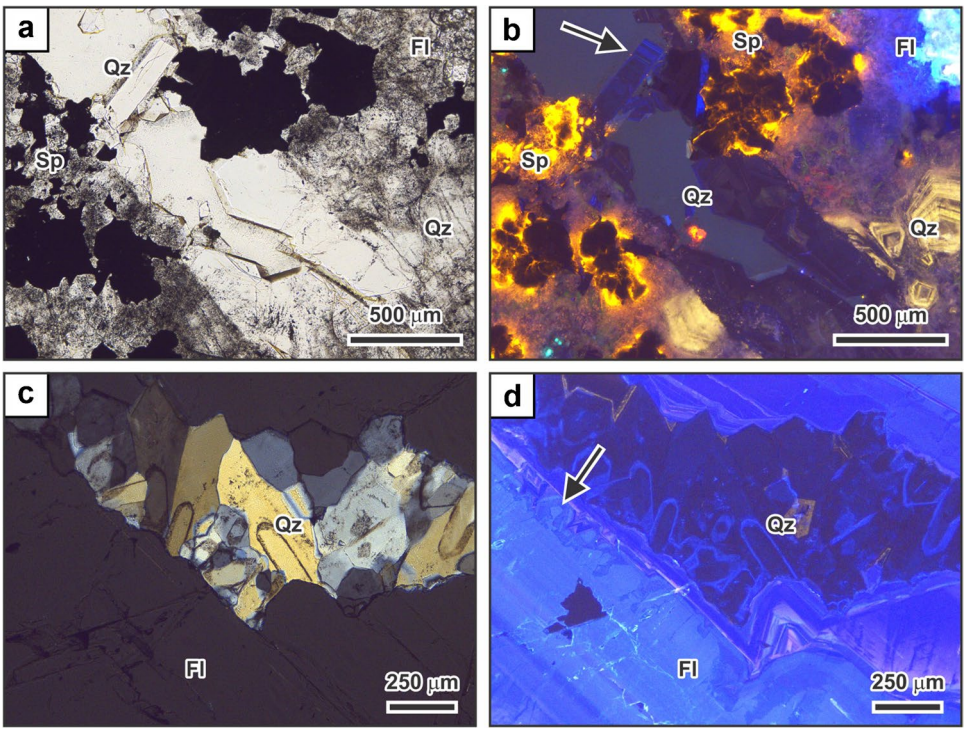

Fig. 11 Textural relationships in post-ore stage veins from the Sunnyside deposit. **a** Euhedral quartz in a fracture that crosscuts an ore mineral dendrite hosted by quartz formed through recrystallization from a noncrystalline precursor. The euhedral quartz crystals are clear and contain comparably few inclusions. Plane polarized light. Sample SUN-2150-D. **b** Corresponding cathodoluminescence (CL) image. The late quartz is characterized by a dark blue to purple CL color and shows growth zoning, including fine oscillatory zoning (arrow). The prismatic quartz formed through recrystallization of a noncrystalline silica precursor is distinctly different from the crosscutting later euhedral quartz. The sphalerite is Fe-poor and exhibits a bright orange to yellow CL color. **c** Post-ore stage fluorite aggregate crosscut by a fracture with drusy quartz. Crossed-polarized light. Sample SUN-2150-3. **d** Corresponding CL image. The euhedral quartz crystals exhibit a dark blue emission during electron bombardment and show faint growth zoning. The fluorite exhibits a bright blue CL and shows complex internal textures, including etch pits along individual growth zones (arrow). Fl fluorite, Qz quartz

temperatures of homogenization were obtained at E level at 3581 msl where a fluid inclusion assemblage yielded 335–340 °C and a salinity of 2.6−3.4 wt% NaCl equiv. The highest homogenization temperature in a sample from D level located at an elevation of 3630 msl was 330–335 °C. This assemblage contained a salinity of 1.7−2.6 wt% NaCl equiv. (Table 1). Clathrate formation was not observed during freezing of the high-temperature inclusions suggesting that CO_2 and other gases are not a major component of the fluid inclusions measured.

Discussion

Gangue and ore mineral textures of the ore-stage veins

The results of this study suggest that essentially all quartz in the ore-stage veins at Sunnyside formed because of recrystallization and maturation of a noncrystalline silica precursor. This conclusion is supported by a comparison between the textures observed at Sunnyside with those documented by previous workers in other epithermal deposits (Sander and Black 1988; Dong et al. 1995; Moncada et al. 2012, 2017; Taksavasu et al. 2018; Tharalson et al. 2019, 2023; Terry et al. 2021; Monecke et al. 2023; Gissler et al. 2024). At Sunnyside, maturation of the noncrystalline silica originally present in the ore-stage veins has progressed to flamboyant or prismatic quartz as the vein material no longer contains an isotropic silica phase.

At the < 2.2 Ma McLaughlin low-sulfidation epithermal deposit in California, opaline veins contain abundant opal-A_G forming microspheres having diameters of 1–5 µm (Monecke et al. 2023; Gissler et al. 2024). The opal- A_G at McLaughlin is only partially transformed to opal-CT and quartz, which allowed identification of textures that record this transition (Gissler et al. 2024). A similar transformation of thermodynamically unstable opal-A_G to quartz has been documented to occur in silica scales and sinter deposits in modern geothermal systems (Campbell et al. 2001; Reyes

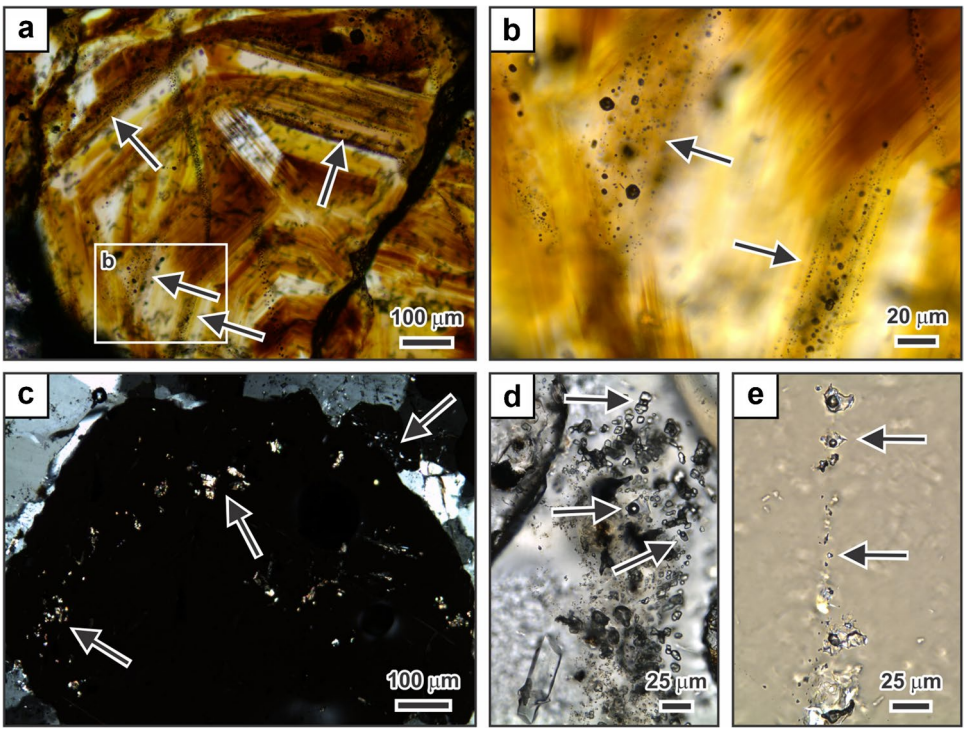

Fig. 12 Photomicrographs of fluid inclusion assemblages in sphalerite and fluorite within post-ore stage veins at the Sunnyside deposit. **a** Euhedral sphalerite crystal containing primary growth zones (arrows) defined by the presence of primary liquid-rich fluid inclusions. Plane polarized light. Sample V244-15. **b** High-magnification image of primary liquid-rich fluid inclusions occurring within two separate growth zones. These growth zones yielded homogenization temperatures of 305–310 °C and salinities of 2.6–3.4 wt% NaCl equiv. **c** Low magnification image of growth zones in fluorite. Primary fluid inclusions in inner growth zones in the sample (two arrows on the left) occur with small, encapsulated rhombic carbonate crystals. In outer growth zones (arrow in the upper right) primary fluid inclusions occur with encapsulated white mica flakes. Crossed-polarized light. Sample SUN-2150-3. **d** High-magnification image of an inner growth zone in a fluorite crystal that contains encapsulated rhomb-shaped carbonate crystals and liquid-rich fluid inclusions showing smooth surfaces and equant shapes. The inclusions have consistent liquid to vapor volumetric proportions. Fluid inclusion assemblages in similar inner growth zones in the sample yielded homogenization temperature of 265–280 °C and salinities of < 1.0 wt% NaCl equiv. Plane polarized light. Sample SUN-2150-3. **e** High-magnification image of an outer growth zone in a fluorite crystal. The zone is defined by liquid-rich fluid inclusions that have consistent liquid to vapor volumetric proportions (arrows) and either adhered to the small, encapsulated mica flakes or completely enclose them. The fluid inclusions show irregular surfaces and shapes. Fluid inclusion assemblages in these outer growth zones in the sample yielded lower homogenization temperatures of 210–250 °C and have salinities of < 1.0 wt% NaCl equiv. Partially crossed-polarized light. Sample SUN-2150-3

et al. 2002; Lynne and Campbell 2004; Rodgers et al. 2004; Raymond et al. 2005; Lynne et al. 2005; Jones 2021).

The study at McLaughlin showed that mosaic quartz, which consists of fine-grained quartz showing interpenetrating grain boundaries, commonly develops during recrystallization of opal-A_G to quartz (Gissler et al. 2024), confirming the results of earlier textural studies documenting the occurrence of mosaic quartz in epithermal veins (Dong et al. 1995; Moncada et al. 2012, 2017; Taksavasu et al. 2018; Tharalson et al. 2019, 2023; Terry et al. 2021). At Sunnyside, this type of quartz is abundant in the ore-stage veins (Fig. 7a, b). In many of the samples investigated, the fine-grained mosaic quartz has even recrystallized further by a processes of grain boundary area reduction resulting in an adjustment of the shape of the grain boundaries and an increase in grain size. Polygonal quartz aggregates in ore-stage veins at Sunnyside are characterized by triple junctions with interfacial angles of ~ 120 ° (Fig. 7c, d).

Based on the study of the McLaughlin deposit in California, Gissler et al. (2024) also showed that flamboyant quartz aggregates and prismatic quartz crystals with zones having a feathery appearance can originate from recrystallization and maturation of opal-A_G. These quartz textures are common in the ore-stage veins at Sunnyside, with prismatic quartz (Figs. 8 and 10a–c) being a particularly important product of maturation and recrystallization of the noncrystalline silica precursor.

During recrystallization, flamboyant and prismatic quartz entrap fluid inclusions along recrystallization fronts, which can resemble growth zones in zonal quartz grown in open space (Gissler et al. 2024). However, bands of these pseudoprimary fluid inclusions (cf.

Table 1 Summary of fluid inclusion microthermometric data

Sample	Mineral	Vein stage	Location	Type	*N*	T_h (°C)	$T_{m,\ ice}$ (°C)	Salinity (wt% NaCl equiv.)
SM-90-2	Euhedral quartz	Pre-ore stage	2150 vein; between G and F levels (between 3467 and 3528 msl)	P	9	310 to 320	−1.5 to −1.0	1.7 to 2.6
20 SVTN-007	Prismatic quartz	Ore-stage (banded and gold ore)	2150 vein; G level (3467 msl)	S	6	325 to 330	−1.5 to −1.0	1.7 to 2.6
SUN-2150-VN	Prismatic quartz	Ore stage (banded ore)	2150 vein; F level (3528 msl)	S	4	325 to 330	−0.6	1.0
				S	4	335 to 340	−2.5 to −2.0	3.4 to 4.2
				S	4	325 to 330	−1.7	2.9
				S	3	320 to 325	−2.5 to −2.0	3.4 to 4.2
				S	4	340 to 345	−1.5 to −1.0	1.7 to 2.6
				S	8	335 to 340	−1.8	3.1
9–18-6–7	Prismatic quartz	Ore-stage (banded ore)	Spur vein; E level (3581 msl)	S	4	325 to 330	−3.0 to −2.5	4.2 to 5.0
				S	6	320 to 325	nd	
				S	4	320 to 325	nd	
9–20-9-2	Prismatic quartz	Ore-stage (banded ore)	Spur vein; E level (3581 msl)	S	5	335 to 340	−2.0 to −1.5	2.6 to 3.4
				S	4	325 to 330	nd	
				S	4	325 to 330	nd	
7–28-4-1	Prismatic quartz	Ore-stage (banded ore)	2150 vein; D level (3630 msl)	S	3	315 to 320	−1.5 to −1.0	1.7 to 2.6
7–28-4-2	Prismatic quartz	Ore-stage (banded ore)	2150 vein; D level (3630 msl)	S	4	315 to 320	−1.0 to −0.5	0.9 to 1.7
9–14-2-1	Prismatic quartz	Ore-stage (banded ore)	2150 vein; D level (3630 msl)	S	3	325 to 330	−0.5 to 0.0	0.0 to 0.9
9–14-2–3	Prismatic quartz	Ore-stage (banded and manganese ore)	2150 vein; D level (3630 msl)	S	4	330 to 335	−1.5 to −1.0	1.7 to 2.6
V244-15	Sphalerite	Post-ore stage	Drill hole B-1 (3245 msl)	P	6	305 to 310	−2.0 to −1.5	2.6 to 3.4
SUN-2150-3	Fluorite	Post-ore stage	2150 vein; G level (3467 msl)	P-core	5	273 to 278	−0.5 to 0.0	0.0 to 0.9
				P-core	3	270 to 275	−0.5 to 0.0	0.0 to 0.9
				P-core	3	265 to 270	−0.2	0.4
				P-core	3	270 to 275	−0.2	0.4
				P-core	3	270 to 275	−0.5 to 0.0	0.0 to 0.9
				P-core	9	270 to 275	−0.5 to 0.0	0.0 to 0.9
				P-rim	6	245 to 250	−0.5 to 0.0	0.0 to 0.9
				P-rim	5	245 to 250	−0.3	0.5
				P-rim	7	230 to 235	−0.5 to 0.0	0.0 to 0.9
				P-rim	4	225 to 230	−0.5 to 0.0	0.0 to 0.9
				P-rim	6	210 to 220	−0.5 to 0.0	0.0 to 0.9
				P-rim	4	210 to 220	−0.5 to 0.0	0.0 to 0.9
				P-rim	6	215 to 220	−0.5 to 0.0	0.0 to 0.9

Type fluid inclusion type; *P* primary; *P-core* primary inclusions in core of crystals; *P-rim* primary inclusions hosted in outer growth zones of crystals; *S* secondary; *n* number of fluid inclusions in assemblage; T_h final homogenization temperature; $T_{m,\ ice}$ ice-melting temperature; *nd* not determined

Sander and Black 1988) are commonly wavy or curved and cross grain boundaries of prismatic quartz crystals, which also provides evidence for quartz formation through recrystallization of a noncrystalline silica precursor. The fact that these bands of pseudoprimary inclusions are abundant even in the largest prismatic crystals

at Sunnyside suggests that none of the quartz in the ore samples is primary in origin.

At McLaughlin and other low-sulfidation epithermal deposits (Vikre 1985, 2007; Sherlock and Lehrman 1995; Saunders and Schoenly 1995a; Shimizu et al. 1998; Burke et al. 2017; Tharalson et al. 2019, 2023; Monecke et al. 2023; Gissler et al. 2024), the ore minerals form dendritic aggregates within the matrix of noncrystalline silica. The dendrites have a fractal geometry (Saunders and Schoenly 1995b). They have delicate shapes and are multi-branching. Monecke et al. (2023) proposed that the originally gel-like noncrystalline silica provided a framework in which the ore mineral dendrites nucleated and grew. The high permeability of the gel permitted diffusion and advection of metals from the hydrothermal liquids flowing across the top of the silica layers to the sites of crystal growth within the gel.

At Sunnyside, broadly similar textural relationships can be observed. In ore-stage veins, ore mineral aggregates are hosted by a silica matrix that is now recrystallized to quartz. As an intermediate-sulfidation epithermal deposit, the veins at Sunnyside contain a higher amount of base metal sulfides when compared to the low-sulfidation epithermal deposits previously studied (Tharalson et al. 2019, 2023; Monecke et al. 2023; Gissler et al. 2024). At Sunnyside, sulfide dendrites can form massive bands of amalgamated dendrites. The original shapes of the dendrites in these bands have been modified during recrystallization and maturation of the silica host to quartz, which included coarsening of the dendrites.

Mechanisms of ore deposition

The textures of the ore-stage vein material at Sunnyside are distinctly different from those in pre- and post-ore stage veins. The ore minerals within the ore-stage material occur as dendrites whereas the sphalerite and other ore minerals in post-ore stage samples are euhedral crystals that undoubtedly grew in open spaces. Crystal growth experiments show that polycrystalline dendritic aggregates form when liquids are supersaturated in the chemical components making up the growing crystals whereas euhedral single crystals can be synthesized at low degrees of supersaturation (Oaki and Imai 2003).

It is hypothesized here that the dendritic ore minerals in the ore-stage vein material grew at far-from-equilibrium conditions. Such conditions were likely reached during vigorous boiling along the host structures resulting in the formation of large amounts of vapor (Christenson and Hayba 1995). In modern geothermal systems, sulfide scaling commonly occurs where substantial amounts of liquid are converted to vapor due to decreasing pressures (Brown 1986; Clark and Williams-Jones 1990; Hardardóttir et al. 2010; Grant et al. 2020). The vapor generation results in silica and metal supersaturation in the liquid that coexists with the vapor (Brown 1986; Christenson and Hayba 1995).

In contrast to engineered geothermal systems, vigorous vapor production in natural hydrothermal systems may involve rapid pressure changes along the structures controlling fluid upflow, which is widely referred to as flashing (Scott and Watanabe 1998; Moncada et al. 2012; Taksavasu et al. 2018; Tharalson et al. 2019, 2023; Slater et al. 2021; Terry et al. 2021; Monecke et al. 2023). During a flashing event, which may be manifested by a hydrothermal eruption at surface (Hedenquist and Henley 1985), vapor is produced in the upper part of the host structure. As a result, the pressures deeper along the structure drop below hydrostatic conditions. As the lower pressure regime migrates downward, an increasing amount of liquid is converted to vapor at depth and within the surrounding wall rock (Henley and Hughes 2000). Due to the decompression, the two-phase conditions migrate down along the controlling structures to depths in which vapor is not normally present. Following the short-lived flashing events, hydrostatic pressure conditions are reestablished. Deep drilling in geothermal systems shows that hydrostatic fluid pressures can prevail to depths of at least 2–3 km below surface (Fournier 1991).

Christenson and Hayba (1995) demonstrated that metal supersaturation in hydrothermal liquids coexisting with vapor during a flashing event is strongly influenced by the amount of vapor produced. Different ore minerals are stabilized by different percentages of vapor coexisting with the liquid. This may explain why banded ores can develop in epithermal deposits such as Sunnyside, with successive bands differing in their mineralogical compositions. Similarly, the different ore types at Sunnyside may simply represent variations in the depth of flashing and the amount of vapor produced. This interpretation differs from the traditional view that variations in ore mineralogy are caused by changes in fluid composition over time, as represented in paragenetic diagrams.

The nature of the boiling process that prevailed during the ore-stage at Sunnyside differed from gentle boiling that has been previously invoked to be the principal mechanism for metal deposition in epithermal deposits. In gentle boiling, a low amount of vapor is produced. The pressures prevailing at a given location do not change over time (Moncada et al. 2012), resulting in the establishment of a defined boiling horizon in which metal deposition occurs (Simmons and Browne 2000). This contrasts with flash vaporization where metal deposition is not necessarily confined to a particular depth interval (Terry et al. 2021).

Interpretation of fluid inclusion inventory in ore-stage veins

The present study establishes that ore-stage veins were originally composed of noncrystalline silica that hosted the ore mineral dendrites. Not unlike the < 2.2 Ma McLaughlin

low-sulfidation epithermal deposit in California (cf. Gissler et al. 2024), this noncrystalline silica precursor may have originally consisted of silica microspheres. Such a gel-like silica precursor did not contain primary fluid inclusions (Gissler et al. 2024). The present petrographic investigations establish that the ore minerals in ore-stage samples are also devoid of primary fluid inclusions hosted in growth zones. The lack of primary fluid inclusions precludes direct reconstruction of the conditions that caused silica supersaturation in the hydrothermal liquids and deposition of the ore minerals.

Recrystallization of the noncrystalline silica precursor resulted in the formation of flamboyant and large prismatic quartz crystals that may contain bands of pseudoprimary inclusions (Sander and Black 1988). These pseudoprimary inclusions were entrapped along crystallographically controlled recrystallization fronts during the conversion from noncrystalline silica to quartz (Gissler et al. 2024). At Sunnyside, pseudoprimary inclusions are commonly highly irregular in shape and may be empty void spaces or may have liquid water with or without vapor bubbles, both widely varying in volumetric proportions. Such inclusion assemblages are not suitable for the determination of homogenization temperatures, which precludes reconstruction of the conditions that prevailed during recrystallization of the noncrystalline silica precursor.

Prismatic quartz is crosscut by liquid-rich secondary fluid inclusions, with some assemblages showing consistent liquid-to-vapor volumetric proportions (Fig. 10f). Some of these assemblages homogenize at high temperatures suggesting that they were entrapped during ongoing high-temperature hydrothermal activity. This implies that recrystallization of the noncrystalline silica to prismatic quartz occurred rapidly. Experimental studies confirm that recrystallization of noncrystalline silica to quartz may occur in days to months at hydrothermal conditions (Bettermann and Liebau 1975; Oehler 1976).

Although the liquid-rich secondary fluid inclusion assemblages crosscutting the prismatic quartz were entrapped under single-phase conditions, the presence of vapor-rich secondary fluid inclusion assemblages (Fig. 10g) implies that vapor production occurred at some stage after recrystallization of some of the noncrystalline silica. As these fluid inclusions are secondary in nature, it is, however, not possible to determine how much time elapsed between ore deposition in one location in a vein at Sunnyside and the subsequent vapor overprint. However, not unlike the high-temperature liquid-rich inclusions occurring as secondary fluid inclusions in the prismatic quartz, the vapor-rich inclusions formed during the ongoing hydrothermal activity. This provides evidence for the abundant generation of vapor at some stage during the deposit formation.

Screening of the fluid inclusion inventory based on inclusion types could result in the incorrect conclusion that vapor production was not an important process at Sunnyside. The quartz in the ore-stage veins does not contain primary fluid inclusion assemblages suitable for the determination of homogenization temperatures, while pre- and post-ore stage veins contain abundant large primary fluid inclusions that can be easily studied. In these veins, the temperatures were not high enough for vapor production to have occurred and no primary vapor-rich fluid inclusions are present. There is little evidence for the presence of vapor if only primary inclusions are surveyed. However, though the vapor-rich fluid inclusions in the prismatic quartz are secondary in origin, they provide direct evidence for vapor production during the ore-stage hydrothermal activity, as post-ore stage quartz does not contain this inclusion type. In contrast to the previous study by Casadevall and Ohmoto (1977), the results of this study suggest that vapor production was the principal process of ore deposition at Sunnyside.

Location of the paleowater table

Ore-stage samples from various levels within the Sunnyside mine (see Supplementary Information) were carefully inspected as part of this study. The highest temperature secondary fluid inclusion assemblages hosted by prismatic quartz were used for microthermometric investigations (Table 1). The high-temperature secondary fluid inclusions measured were all liquid-rich and did not coexist with vapor-rich inclusions suggesting that they were entrapped under single-phase conditions. As such, the homogenization temperatures recorded for samples from different mine levels must be enveloped by a common boiling curve that separates single-phase from two-phase conditions.

Figure 13 shows the homogenization data of the secondary fluid inclusion assemblages in the samples collected at various levels within the mine. The homogenization temperatures range up to 345 °C in a sample from F level at an elevation of 3528 msl. Assuming a fluid salinity of 2.5 wt% NaCl, all measured homogenization temperatures can be enveloped by a common boiling curve (cf. Haas 1971). The paleowater table corresponding to this boiling curve would have been located at a modern elevation of ~ 5100 msl (Fig. 13). As mineralization at Sunnyside extends vertically for ~ 600 m from an elevation of 3840 msl down to the American Tunnel at 3250 msl, deposit formation occurred at a depth of ~ 1300–1900 m below the paleowater table. This is comparable to the depth at which vapor formation occurs in some modern geothermal systems (Clark and Williams-Jones 1990; Simmons et al. 2007).

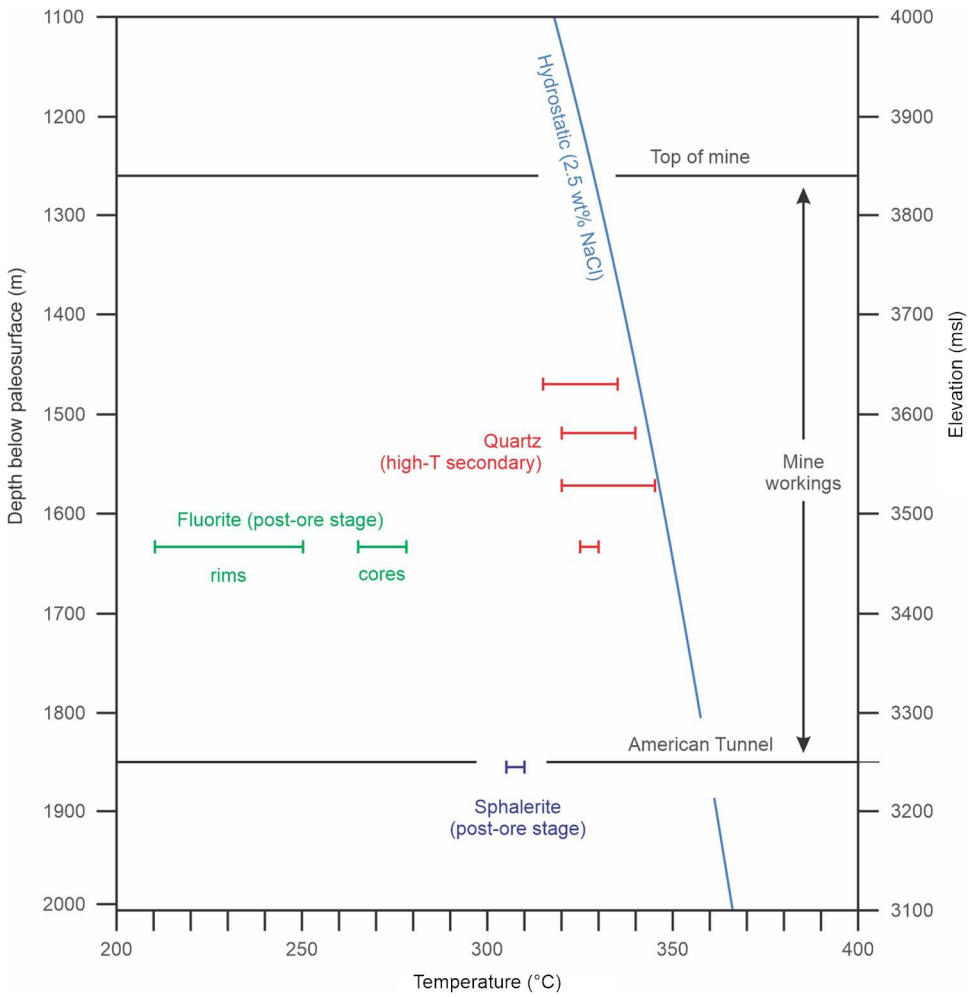

Fig. 13 Reconstruction of the hydrological conditions at the Sunnyside deposit. The plot shows that the highest temperature secondary fluid inclusion assemblages hosted by prismatic quartz in ore-stage vein samples from Sunnyside (red) can be enveloped by the boiling-point-to-depth curve of H_2O containing 2.5 wt% NaCl calculated based on the pressure head exerted by the overlying column of hydrothermal fluid (cf. Haas 1971). The data suggest that the paleosurface would have been located at an elevation of ~ 5100 msl. Homogenization temperature data obtained on primary fluid inclusions hosted by post-ore stage sphalerite (dark blue) and fluorite (green) plot into the single-phase field far away from the boiling-point-to-depth curve. This indicates that post-ore stage minerals formed at the waning stages of the hydrothermal system. Microthermometric data are given in Table 1. Data obtained by Casadevall and Ohmoto (1977) are not plotted because they were not collected with respect to fluid inclusion assemblages

Conceptual model

The Sunnyside intermediate-sulfidation epithermal deposit formed from hydrothermal liquids ascending along extensional structures associated with the Eureka graben. Based on the occurrence of porphyry veins in the deep drill hole below Sunnyside (Guzman et al. 2023) and geophysical imaging (Rodriguez et al. 2024), it is hypothesized that the hydrothermal liquids that caused deposit formation were sourced from a porphyritic intrusion emplaced below the Eureka graben.

Three end-member hydrological conditions existed during the formation of the Sunnyside deposit. During the pre-ore stage at Sunnyside, fluid flow was primarily controlled by networks of microfractures. The volcanic host rocks surrounding these fractures have been affected by silicification and sericite alteration, with pyrite being abundant. Microfractures, narrow veins, and vugs within the altered wall rocks contain small euhedral quartz crystals that grew in open spaces. The quartz crystals contain encapsulated sericite flakes as well as primary, liquid-rich fluid inclusion assemblages. Evidence for the occurrence of boiling such as coexisting liquid- and vapor-rich fluid inclusions have not been identified in this study as well as the previous investigations by Casadevall and Ohmoto (1977). This suggests that formation of the quartz took place from cooling hydrothermal liquids as quartz solubility decreases with temperature in the epithermal environment (Fournier 1985; Monecke et al. 2018).

As the hydrothermal system became established, upflow of high-temperature hydrothermal liquids occurred primarily along major faults. The hydrothermal liquids ascending along these structures experienced short-lived events of flashing, presumably triggered by earthquakes or dike emplacement (Rowland and Simmons 2012; Sanchez-Alfaro et al. 2016, 2024; Amagai et al. 2019). The bulk of the ore at Sunnyside was formed under these conditions with the transitory pressure changes and associated mineral deposition occurring to a depth of ~ 1300–1900 m below the paleowater table. Vapor loss from the hydrothermal liquids caused supersaturation and precipitation of noncrystalline silica. The ore mineral dendrites grew within gel-like silica

matrix, with the amount of vapor produced during a giving flashing event controlling which ore minerals precipitated.

In contrast to the ore-stage, the late veins at Sunnyside are characterized by the presence of abundant euhedral crystals of quartz, fluorite, calcite, and rhodochrosite that have formed in open spaces within the veins (Burbank and Luedke 1969; Casadevall and Ohmoto 1977). Fluid inclusion work of the current study and previous research by Casadevall and Ohmoto (1977) showed that primary inclusions in the fluorite have comparably low homogenization temperatures. No evidence for boiling such as the coexistence liquid-rich and vapor-rich fluid inclusions in a single assemblage (cf. Bodnar et al. 1985), or assemblages of only vapor-rich inclusions (cf. Bodnar et al. 1985), have been identified. Post-ore stage mineral deposition must have occurred because of buoyancy driven hydrothermal fluid flow at quasi steady-state conditions during the waning stages of the hydrothermal system.

The results of this study place the polymetallic veins of the Sunnyside deposit at a depth of ~ 1300–1900 m below the paleowater table, which is deeper than the depth limit of 1500 m that is currently used to define the epithermal environment (Simmons et al. 2005). Fluid temperatures during the formation of the ore-stage were as high as 345 °C. Despite the significant depth of mineralization below the paleosurface and the high temperatures of the hydrothermal liquids, Sunnyside should be classified as an epithermal deposit. The processes of mineralization at Sunnyside are similar to those observed in other epithermal deposits. Several recent studies have established that flashing is common in the epithermal environment (Scott and Watanabe 1998; Koděra et al. 2005; Moncada et al. 2012, 2017; Taksavasu et al. 2018; Tharalson et al. 2019, 2023; Slater et al. 2021; Terry et al. 2021; Monecke et al. 2023).

The Western San Juan Mountains are host to a large number of polymetallic vein deposits in an area that has a NW-SE extent of ~ 20 km and a NE-SW extent of ~ 25 km, which is comparable in size to world-class epithermal districts worldwide (Simmons et al. 2005). In addition to Sunnyside, other important deposits include the Gold King (Burbank 1951; Taylor 1988; Free et al. 1990; Koch 1990) in the Eureka district, the Camp Bird, Idarado, and Revenue-Virginius deposits near Telluride (Spurr 1925; Mayor and Fisher 1972; Paul 1974; Coxe 1985; Barratt 1990; Fisher 1990; Parsons et al. 2022), and the Shenandoah-Dives deposit in the South Silverton district (Ransome 1901; Varnes 1963; Hardwick 1984; Bove et al. 2007). These polymetallic vein deposits are likely all intermediate-sulfidation epithermal deposits although only few studies have attempted to constrain the depth of mineralization below the paleowater table in the deposits of the Western San Juan Mountains (Nash 1975; Casadevall and Ohmoto 1977; Barratt 1990). The deposits have similar hydrological histories involving formation of early barren quartz-pyrite veins, followed by the ore-stage veins, and a final stage of quartz, fluorite, and carbonate minerals formed in open spaces (Ransome 1901; Hulin 1929; Burbank 1933; Burbank and Luedke 1969; Casadevall and Ohmoto 1977; Taylor 1988; Bartos 1993). The widespread occurrence of banded ores and crustiform textures (Ransome 1901; Hillebrand 1968; Burbank and Luedke 1969; Coxe 1985; Taylor 1988; Barratt 1990; Bartos 1993) suggests that flashing may have been the principal process of mineral deposition during the ore stage in all these intermediate-sulfidation epithermal deposits.

Conclusions

This study provides an update on previous research at the Sunnyside deposit in the San Juan Mountains of Colorado using a modern ore deposit framework. Although previous studies have described the mineralogy of the epithermal veins at Sunnyside, the processes of mineral deposition were only poorly constrained. The present study shows that the microtextural characteristics of ore-stage veins are complicated as essentially all quartz in these veins has formed through recrystallization of a noncrystalline silica precursor. This silica precursor and the ore minerals grown in the silica matrix do not contain primary fluid inclusion assemblages precluding direct reconstruction of the conditions of vein formation. However, microthermometric measurements on high-temperature, liquid-rich secondary fluid inclusion assemblages crosscutting quartz formed through recrystallization, as well as the occurrence of vapor-rich inclusions in this quartz type, show that the hydrothermal liquids experienced vapor loss during the ore-stage. The conditions that prevailed during the ore-stage differ significantly from those during the pre-ore and post-ore stage vein formation when the hydrothermal system was waxing and waning, respectively. During these times, cooling of the ascending hydrothermal fluids resulted in the widespread formation of gangue minerals in open spaces, which contain primary fluid inclusion assemblages entrapped at conditions below the boiling-point-to-depth curve.

The textural evidence suggests that mineral deposition during the ore-stage occurred at far-from-equilibrium conditions, presumably during short-lived events of flashing of the hydrothermal liquids. Flash vaporization of the hydrothermal liquids would have resulted in rapid supersaturation of silica and metals in the remaining liquid, promoting formation of ore mineral dendrites in the originally noncrystalline silica matrix. The findings of this study may have significant implications to the understanding of ore-forming processes in the epithermal environment. It is demonstrated that textural studies may provide important insights into the processes of mineral deposition that cannot be readily gained through fluid inclusion studies.

Supplementary Information The online version contains supplementary material available at https://doi.org/10.1007/s00126-024-01341-9.

Acknowledgements We thank Thomas Casadevall, scientist emeritus at the U.S. Geological Survey, for contributing samples from the Sunnyside deposit for this study and for providing valuable insights into the deposit geology. Several additional samples, originally collected by Steve Vennis in 1988−1989, were provided by Bob Stoufer. We are grateful to Eric Anderson and Douglas Yager of the U.S. Geological Survey for assisting during field work at Sunnyside and discussions on the geology and geophysics of the Sunnyside deposit and the Eureka graben. We thank James Hagadorn from the Denver Museum of Nature and Science for providing access to sample material from Sunnyside, including rhodochrosite samples of the post-ore stage. We thank Daniel Moncada and an anonymous reviewer for their constructive reviews of an earlier version of this contribution.

Funding information This research was supported by the U.S. Geological Survey Mineral Resources Program and the Society of Economic Geologist Hugh McKinstry Student Research Grant. TM acknowledges funding by the National Science Foundation (NSF) that supports operation of the Center to Advance the Science of Exploration to Reclamation in Mining, which is a joint industry-university collaborative research center between the Colorado School of Mines and Virginia Tech under NSF award numbers 1822146 and 1822108.

Declarations

Conflict of interest The authors declare no competing interests.

References

Albinson T, Norman DI, Cole D, Chomiak B (2001) Controls on formation of low-sulfidation epithermal deposits in Mexico: constraints from fluid inclusion and stable isotope data. SEG Spec Pub 8:1–32

Amagai T, Okamoto A, Niibe T, Hirano N, Motomiya K, Tsuchiya N (2019) Silica nanoparticles produced by explosive flash vaporization during earthquakes. Sci Rep 9:9738

Barratt RM (1990) Gold in the Camp Bird vein system, southwestern Colorado. MS thesis, Colorado School of Mines

Bartos PJ (1993) Comparison of gold-rich and gold-poor quartz-base metal veins – Western San Juan Mountains, Colorado: the Mineral Point area as an example. SEG Newsl 15(1):6–11

Best MG, Christiansen EH, de Silva S, Lipman PW (2016) Slab-rollback ignimbrite flareups in the southern Great Basin and other cenozoic American arcs: a distinct style of arc volcanism. Geosphere 12:1097–1135

Bettermann P, Liebau F (1975) The transformation of amorphous silica to crystalline silica under hydrothermal conditions. Contrib Mineral Petrol 53:25–36

Blood WA (1968) Geology, history, and economics of the Sunnyside mine, Eureka mining district, San Juan County, Colorado. PhD thesis, Colorado School of Mines

Bodnar RJ, Reynolds TJ, Kuehn CA (1985) Fluid-inclusion systematics in epithermal systems. Rev Econ Geol 2:73–97

Bodnar RJ, Vityk MO (1994) Interpretation of microthermometric data for H_2O-NaCl fluid inclusions. In: De Vivo B, Frezzotti ML (eds) Fluid inclusions in minerals, methods and applications. Virginia Tech, Blacksburg, pp 117–130

Bove DJ, Hon K, Budding KE, Slack JF, Snee LW, Yeoman RA (2001) Geochronology and geology of late Oligocene through Miocene Volcanism and mineralization in the Western San Juan Mountains, Colorado. USGS Prof Pap 1642:30

Bove DJ, Mast MA, Dalton JB, Wright WG, Yager DB (2007) Major styles of mineralization and hydrothermal alteration and related solid- and aqueous-phase geochemical signatures. USGS Prof Pap 1651:165–230

Brown KL (1986) Gold deposition from geothermal discharges in New Zealand. Econ Geol 81:979–983

Buchanan LJ (1981) Precious metal deposits associated with volcanic environments in the Southwest. Arizona Geol Soc Digest 14:237–262

Burbank WS (1933) The manganese minerals of the Sunnyside veins, Eureka Gulch, Colorado. Am Mineral 18:513–527

Burbank WS (1951) The Sunnyside, Ross Basin, and Bonita fault systems and their associated ore deposits, San Juan County, Colorado. Colo Sci Soc Proc 15:285–304

Burbank WS (1960) Pre-ore propylitization, Silverton caldera, Colorado. USGS Prof Pap 400–B:B12–B13

Burbank WS, Luedke RG (1969) Geology and ore deposits of the Eureka and adjoining districts, San Juan Mountains, Colorado. USGS Prof Pap 535:73

Burke M, Rakovan J, Krekeler MPS (2017) A study by electron microscopy of gold and associated minerals from Round Mountain, Nevada. Ore Geol Rev 91:708–717

Campbell KA, Sannazzaro K, Rodgers KA, Herdianita NR, Browne PRL (2001) Sedimentary facies and mineralogy of the late Pleistocene Umukuri silica sinter, Taupo Volcanic Zone, New Zealand. J Sed Res 71:727–746

Camprubí A, Albinson T (2007) Epithermal deposits in México — update of current knowledge, and an empirical reclassification. Geol Soc Amer Spec Pap 422:377–415

Casadevall T, Ohmoto H (1977) Sunnyside mine, Eureka mining district, San Juan County, Colorado: geochemistry of gold and base metal ore deposition in a volcanic environment. Econ Geol 72:1285–1320

Christenson BW, Hayba DO (1995) Hydrothermal eruptions in ore forming reservoirs: analogues and models. Proceedings of the PACRIM Congress, Auckland, New Zealand, pp 119–124

Clark JR, Williams-Jones AE (1990) Analogues of epithermal gold-silver deposition in geothermal well scales. Nature 346:644–645

Claveria RJR (2001) Mineral paragenesis of the Lepanto copper and gold and the Victoria gold deposits, mankayan mineral district, Philippines. Resour Geol 51:97–106

Coxe BW (1985) The Virginius vein ore deposit, northwestern San Juan Mountains, Colorado: a study of the mineralogy, structure, and fluid inclusions of an epithermal base-metal and silver vein in a volcanic environment. MS thesis, University of New Mexico Albuquerque

Dong G, Morrison G, Jaireth S (1995) Quartz textures in epithermal veins, Queensland – classification, origin, and implication. Econ Geol 90:1841–1856

Drummond SE, Ohmoto H (1985) Chemical evolution and mineral deposition in boiling hydrothermal systems. Econ Geol 80:126–147

Einaudi MT, Hedenquist JW, Inan EE (2003) Sulfidation state of fluids in active and extinct hydrothermal systems: transitions from porphyry to epithermal environments. SEG Spec Pub 10:285–313

Fisher FS (1990) Gold deposits in the sneffels-Telluride and Camp Bird mining districts, San Juan Mountains, Colorado. USGS Bull 1857–F:12–18

Fournier RO (1985) The behavior of silica in hydrothermal solutions. Rev Econ Geol 2:45–61

Fournier RO (1991) The transition from hydrostatic to greater than hydrostatic fluid pressure in presently active continental hydrothermal systems in crystalline rock. Geophys Res Lett 18:955–958

Free B, Hutchinson RW, Koch BC (1990) Gold deposition at Gold King, Silverton Caldera, Colorado. Mitt Naturwiss Ver Steiermark 120:135–143

Geology Staff Sunnyside Gold Corporation (1988) Structure & ore deposits of the Sunnyside mine, Silverton, Colorado. SEG Guideb Ser 3:61–73

Gissler GD, Monecke T, Reynolds TJ, Guzman MA, Ellison ET, Sherlock R (2024) Microtextural evidence for the recrystallization of opal-A to quartz in epithermal veins: a case study from the McLaughlin deposit, California. Ore Geol Rev 169:106105

Goldstein RH, Reynolds TJ (1994) Systematics of fluid inclusions in diagenetic minerals. SEPM Short Course 31:198

Gonzales DA (2015) New U-Pb zircon and $^{40}Ar/^{39}Ag$ age constraints on the late mesozoic to cenozoic plutonic record in the Western San Juan Mountains. Mountain Geol 52:5–42

Grant HLJ, Hannington MD, Hardardóttir V, Fuchs SH, Schumann D (2020) Trace metal distributions in sulfide scales of the seawater-dominated Reykjanes geothermal system: constraints on sub-seafloor hydrothermal mineralizing processes and metal fluxes. Ore Geol Rev 116:103145

Guzman M, Monecke T, Reynolds TJ, Casadevall T (2023) Evidence for a high-level porphyritic intrusion below the Sunnyside epithermal vein deposit, Colorado. In: Proceedings of the 17th Biennial Meeting of the Society for Geology Applied to Mineral Deposits, Zürich, Switzerland, pp 56–59

Haas JL Jr (1971) The effect of salinity on the maximum thermal gradient of a hydrothermal system at hydrostatic pressure. Econ Geol 66:940–946

Hardardóttir V, Hannington M, Hedenquist J, Kjarsgaard I, Hoal K (2010) Cu-rich scales in the reykjanes geothermal system, Iceland. Econ Geol 105:1143–1155

Hardwick JF (1984) Epithermal vein and carbonate replacement mineralization related to caldera development, Cunningham Gulch, Silverton, Colorado. MA thesis, University of Texas at Austin

Hayba DO (1997) Environment of ore deposition in the Creede mining district, San Juan Mountains, Colorado: part V. Epithermal mineralization from fluid mixing in the OH vein. Econ Geol 92:29–44

Hedenquist JW, Henley RW (1985) Hydrothermal eruptions in the Waiotapu geothermal system, New Zealand: their origin, associated breccias, and relation to precious metal mineralization. Econ Geol 80:1640–1668

Hedenquist JW, Arribas A, Gonzalez-Urien E (2000) Exploration for epithermal gold deposits. SEG Rev 13:245–277

Henley RW, Hughes GO (2000) Underground fumaroles: excess heat effects in vein formation. Econ Geol 95:453–466

Hillebrand JR (1968) The Idarado mine. In: New Mexico Geol Soc 19th Ann Fall Field Conf Guideb 130–140

Hulin CD (1929) Structural control of ore deposition. Econ Geol 24:15–49

John DA (2001) Miocene and early Pliocene epithermal gold-silver deposits in the northern Great Basin, western United States: characteristics, distribution, and relationship to magmatism. Econ Geol 96:1827–1853

John DA, Garside LJ, Wallace AR (1999) Magmatic and tectonic setting of late cenozoic epithermal gold-silver deposits in northern Nevada, with an emphasis on the Pah Rah and Virginia ranges and the Northern Nevada Rift. Geol Soc Nev Spec Pub 29:65–158

Jones B (2021) Siliceous sinters in thermal spring systems: review of their mineralogy, diagenesis, and fabrics. Sediment Geol 413:105820

Kamilli RJ, Ohmoto H (1977) Paragenesis, zoning, fluid inclusion, and isotopic studies of the Finlandia vein, Colqui district, central Peru. Econ Geol 72:950–982

Koch BC (1990) Origin of the Gold King-Davis epithermal gold lode, Silverton caldera, Colorado. PhD thesis, Colorado School of Mines

Koděra P, Lexa J, Rankin AH, Fallick AE (2005) Epithermal gold veins in a caldera setting: Banská Hodruša, Slovakia. Min Depos 39:921–943

Langston DJ (1978) The geology and geochemistry of the northeasterly gold veins, Sunnyside mine, San Juan County, Colorado. MS thesis, Colorado School of Mines

Leary S, Sillitoe RH, Stewart PW, Roa KJ, Nicolson BE (2016) Discovery, geology, and origin of the Fruta Del Norte Epithermal gold-silver deposit, southeastern Ecuador. Econ Geol 111:1043–1072

Lipman PW (1975) Evolution of the Platoro caldera complex and related volcanic rocks, southeastern San Juan Mountains, Colorado. USGS Prof Pap 852:128

Lipman PW (1976) Geologic map of the Lake City caldera area, Western San Juan Mountains, southwestern Colorado. USGS Misc Investig Ser Map I -962, scale 1:48,000

Lipman PW (2007) Incremental assembly and prolonged consolidation of Cordilleran magma chambers: evidence from the Southern Rocky Mountain volcanic field. Geosphere 3:42–70

Lipman PW, Bachmann O (2015) Ignimbrites to batholiths: integrating perspectives from geological, geophysical, and geochronological data. Geosphere 11:705–743

Lipman PW, Steven TA, Luedke RG, Burbank WS (1973) Revised volcanic history of the San Juan, Uncompahgre, Silverton, and Lake City calderas in the Western San Juan Mountains, Colorado. J Res USGS 1:627–642

Lipman PW, Zimmerer MJ, McIntosh WC (2015) An ignimbrite caldera from the bottom up: exhumed floor and fill of the resurgent Bonanza caldera, Southern Rocky Mountain volcanic field. Colo Geosph 11:1902–1947

Lynne BY, Campbell KA (2004) Morphologic and mineralogic transitions from opal-A to opal-CT in low-temperature siliceous sinter diagenesis, Taupo Volcanic Zone, New Zealand. J Sed Res 74:561–579

Lynne BY, Campbell KA, Moore JN, Browne PRL (2005) Diagenesis of 1900-year-old siliceous sinter (opal-A to quartz) at Opal Mound, Roosevelt Hot Springs, Utah, U.S.A. Sediment Geol 179:249–278

Mayor JN, Fisher FS (1972) Middle Tertiary replacement ore bodies and associated veins in the northwest San Juan Mountains, Colorado. Econ Geol 67:214–230

McIntosh WC, Chapin CE (2004) Geochronology of the central Colorado volcanic field. NMBGMR Bull 160:205–237

Moncada D, Mutchler S, Nieto A, Reynolds TJ, Rimstidt JD, Bodnar RJ (2012) Mineral textures and fluid inclusion petrography of the epithermal Ag–Au deposits at Guanajuato, Mexico: application to exploration. J Geochem Explor 114:20–35

Moncada D, Baker D, Bodnar RJ (2017) Mineralogical, petrographic and fluid inclusion evidence for the link between boiling and epithermal Ag-Au mineralization in the La Luz area, Guanajuato mining district, México. Ore Geol Rev 89:143–170

Monecke T, Monecke J, Reynolds TJ, Tsuruoka S, Bennett MM, Skewes WB, Palin RM (2018) Quartz solubility in the H_2O-NaCl system: a framework for understanding vein formation in porphyry copper deposits. Econ Geol 113:1007–1046

Monecke T, Reynolds TJ, Taksavasu T, Tharalson ER, Zeeck LR, Guzman M, Gissler G, Sherlock R (2023) Natural growth of gold dendrites within silica gels. Geology 51:189–192

Nash JT (1975) Fluid inclusion studies of vein, pipe, and replacement deposits, northwestern San Juan Mountains, Colorado. Econ Geol 70:1448–1462

Neuser RD (1995) A new high-intensity cathodoluminescence microscope and its application to weakly luminescing minerals. Bochum Geol Geotechn Arb 44:116–118

Oaki Y, Imai H (2003) Experimental demonstration for the morphological evolution of crystals grown in gel media. Cryst Growth Des 3:711–716

Oehler JH (1976) Hydrothermal crystallization of silica gel. Geol Soc Am Bull 87:1143–1152

Parsons B, Olin EJ, Tinucci J, Osborn J, Prosser B, Poeck J, Braun T (2022) NI 43–101 Technical report feasibility study: Revenue-Virginius mine, Ouray, Colorado. Report prepared by SRK Consulting, Denver

Paul AH (1974) Geology and ore deposits of the Camp Bird mine, Ouray County, Colorado. MS thesis, Colorado School of Mines

Ransome FL (1901) A report on the economic geology of the Silverton Quadrangle. Colo USGS Bull 182:265

Raymond J, Williams-Jones AE, Clark JR (2005) Mineralization associated with scale and altered rock and pipe fragments from the Berlín geothermal field, El Salvador; implications for metal transport in natural systems. J Volcanol Geotherm Res 145:81–96

Reed MH (1997) Hydrothermal alteration and its relationship to ore fluid composition. In: Barnes HL (ed) Geochemistry of hydrothermal ore deposits, 3rd edn. Wiley, New York, pp 303–365

Reyes AG, Trompetter WJ, Britten K, Searle J (2002) Mineral deposits in the Rotokawa geothermal pipelines, New Zealand. J Volcanol Geotherm Res 119:215–239

Rodgers KA, Browne PRL, Buddle TF, Cook KL, Greatrex RA, Hampton WA, Herdianita NR, Holland GR, Lynne BY, Martin R, Newton Z, Pastars D, Sannazarro KL, Teece CIA (2004) Silica phases in sinters and residues from geothermal fields of New Zealand. Earth-Sci Rev 66:1–61

Rodriguez BD, Yager DB, Anderson ED, Hoogenboom BE, Runkel RL, Smith BD, Deszcz-Pan M (2024) Deep resistivity geophysics of the San Juan-Silverton caldera complex, San Juan County, Colorado (USA). Geosph 20:910–934

Rowland JV, Simmons SF (2012) Hydrologic, magmatic, and tectonic controls on hydrothermal flow, Taupo Volcanic Zone, New Zealand: implications for the formation of epithermal vein deposits. Econ Geol 107:427–457

Sanchez-Alfaro P, Reich M, Driesner T, Cembrano J, Arancibia G, Pérez-Flores P, Heinrich CA, Rowland J, Tardani D, Lange D, Campos E (2016) The optimal windows for seismically-enhanced gold precipitation in the epithermal environment. Ore Geol Rev 79:463–473

Sanchez-Alfaro P, Wallis I, Iturrieta P, Rowland J, Dempsey D, O'Sullivan J, Reich M, Cembrano J (2024) Earthquakes trigger rapid flash boiling front at optimal geologic conditions. Geophys Res Lett 51, e2023GL108109

Sander MV, Black JE (1988) Crystallization and recrystallization of growth-zoned vein quartz crystals from epithermal systems — implications for fluid inclusion studies. Econ Geol 83:1052–1060

Saunders JA, Schoenly PA (1995a) Boiling, colloid nucleation and aggregation, and the genesis of bonanza Au-Ag ores of the Sleeper deposit, Nevada. Min Depos 30:199–210

Saunders JA, Schoenly PA (1995b) Fractal structure of electrum dendrites in bonanza epithermal Au-Ag deposits. In: Barton CC, La Pointe PR (eds) Fractals in the earth sciences. Springer, New York, pp 251–261

Scott AM, Watanabe Y (1998) Extreme boiling model for variable salinity of the Hokko low-sulfidation epithermal au prospect, southwestern Hokkaido, Japan. Min Depos 33:568–578

Sherlock RL, Lehrman NJ (1995) Occurrences of dendritic gold at the McLaughlin mine hot-spring gold deposit. Min Depos 30:323–327

Shimizu T, Matsueda H, Ishiyama D, Matsubaya O (1998) Genesis of epithermal Au-Ag mineralization of the Koryu Mine, Hokkaido, Japan. Econ Geol 93:303–325

Sillitoe RH (2010) Porphyry copper systems. Econ Geol 105:3–41

Sillitoe RH, Hedenquist JW (2003) Linkages between volcanotectonic settings, ore-fluid compositions, and epithermal precious metal deposits. SEG Spec Pub 10:315–343

Simmons SF, Browne PRL (2000) Hydrothermal minerals and precious metals in the Broadlands-Ohaaki geothermal system: implications for understanding low-sulfidation epithermal environments. Econ Geol 95:971–999

Simmons SF, Gemmell JB, Sawkins FJ (1988) The Santo Niño silver-lead-zinc vein, Fresnillo district, Zacatecas, Mexico: part II. Physical and chemical nature of ore-forming solutions. Econ Geol 83:1619–1641

Simmons SF, White NC, John DA (2005) Geological characteristics of epithermal precious and base metal deposits. In: Hedenquist JW, Thompson JFH, Goldfarb RJ, Richards JP (eds) Economic geology 100th anniversary volume. Society of Economic Geologists, Littleton, pp 485–522

Simmons SF, Simpson MP, Reynolds TJ (2007) The significance of clathrates in fluid inclusions and the evidence for overpressuring in the Broadlands-Ohaaki geothermal system, New Zealand. Econ Geol 102:127–135

Slater ET, Kontak DJ, Mcdonald AM, Fayek M (2021) Origin of a multi-stage epithermal Ag-Zn-Pb-Sn deposit: the Miocene cortaderas breccia body, Pirquitas mine, NW Argentina. Min Depos 56:381–406

Spurr JE (1925) The Camp Bird compound veindike. Econ Geol 20:115–152

Standen AR, Kyle JR (1985) Geologic characteristics of the Scotia-Vanderbilt vein, Silverton, Colorado: implications for epithermal precious metal exploration in volcanic settings. In: Second International Congress on Applied Mineralogy in the Minerals Industry, Los Angeles, California, pp 1051–1063

Steven TA, Lipman PW (1976) Calderas of the San Juan Volcanic Field, southwestern Colorado. USGS Prof Pap 958:35

Taksavasu T, Monecke T, Reynolds TJ (2018) Textural characteristics of noncrystalline silica in sinters and quartz veins: implications for the formation of bonanza veins in low-sulfidation epithermal deposits. Minerals 8:331

Taylor FD (1988) Geology and ore deposits of the Gold King mine, Eureka mining district, San Juan County, Colorado. SEG Guideb Ser 3:74–88

Terry LR, Monecke T, Reynolds TJ, Tharalson ER, Pfaff K, Kelly NM, Hennigh QT (2021) Textural characteristics of barren and mineralized colloform quartz bands at the low-sulfidation epithermal deposits of the Omu camp in Hokkaido, Japan: implications for processes resulting in bonanza-grade precious metal enrichment. Econ Geol 116:407–425

Tharalson ER, Monecke T, Reynolds TJ, Zeeck L, Pfaff K, Kelly NM (2019) The distribution of precious metals in high-grade banded quartz veins from low-sulfidation epithermal deposits: constraints from μXRF mapping. Minerals 9:740

Tharalson ER, Taksavasu T, Monecke T, Reynolds TJ, Kelly NM, Pfaff K, Bell AS, Sherlock R (2023) Textural characteristics of ore mineral dendrites in banded quartz veins from low-sulfidation epithermal deposits: implications for the formation of bonanza-type precious metal enrichment. Min Depos 58:1395–1419

Varnes DJ (1963) Geology and ore deposits of the south Silverton mining area, San Juan County, Colorado. USGS Prof Pap 378–A:56

Vikre PG (1985) Precious metal vein systems in the National district, Humboldt County, Nevada. Econ Geol 80:360–393

Vikre PG (1989) Fluid-mineral relations in the Comstock Lode. Econ Geol 84:1574–1613

Vikre PG (2007) Sinter-vein correlations at Buckskin Mountain, National district, Humboldt County, Nevada. Econ Geol 102:193–224

Waegli JA (1979) Geology and mineralization of the Uncle Sam vein and surrounding area, San Juan County, Colorado. MS thesis, Colorado School of Mines

Wang L, Qin KZ, Song GX, Li GM (2019) A review of intermediate sulfidation epithermal deposits and subclassification. Ore Geol Rev 107:434–456

Yager DB, Bove DJ (2002) Generalized geologic map of part of the upper Animas River watershed and vicinity, Silverton, Colorado. USGS Misc Field Studies Map MF-2377, scale 1:48,000